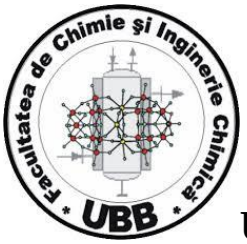

UNIVERSITY BABEȘ-BOLYAI

FACULTY DE CHEMISTRY AND CHEMICAL ENGINEERING

PHD THESIS ABSTRACT

ADVANCED BIOMATERIALS BASED ON BIOACTIVE INORGANIC POWDERS AND NATURAL OR SYNTHETIC POLYMERIC MATRICES WITH APPLICATIONS IN MEDICINE

PHD STUDENT: Ioana-Maria Hodișan (Ambrosie)

SUPERVISOR: Prof. Univ. Dr. Maria Tomoaia-Cotișel

Cluj-Napoca

2018

KEY WORDS: GIOMER, PRE-REACTED GLASS, INORGANIC FILLER, RESIN MATRIX, ADHESION, ADHESIVE SYSTEMS, LOCK-IN THERMOGRAPHY, AFM, SEM, BIOCOMPATIBILITY

Contents

Chapter 1. Advanced biomaterials for use in medicine

1.1 Biomaterials for the restoration, regeneration and remineralisation of dental tissues

Research studies in the field of restorative dentistry in the last decades have focused on finding an ideal restoration material as an alternative to silver amalgam.

This need for replacement led to the development of new classes of restoration materials, of which composite resins took the first place. Between 1958 and 1962, Bowen, through the discovery of the Bis-GMA monomer, laid the foundation for the development of a new class of adhesive resins, now known as diacrylic resins, which may be simple (unfilled diacrylic resins) or composites (with inorganic filler). [1], [2]. Diacrylic resins today have a wide spread in all branches of adhesive dentistry (odontology, periodontics, orthodontics, prosthetics, surgery) due to their adhesion to dental and other substrates through adhesive systems.

As an alternative to composite resins, a new class of dental restorative materials has been developed: glass ionomer cements (GIC). These were introduced on the market in 1970 following research by Wilson and Kent by Dentsply and ESPE. They are a mixture of alumino-floro-silicate calcium glass with polycarboxylic acids. The advantages of this class of restoration materials are increased biocompatibility, chemical adhesion to dental tissues without the need for an adhesive system, lack of polymerization contraction, release of fluoride ions initiating remineralization of dental tissues.

After careful observation of these two classes of materials, diacrylic resins and glass ionomer cements, the attention was focused on obtaining hybrid materials that take over the advantages of both classes of materials and annihilate or reduce their disadvantages. Thus, resin-modified glass ionomer cements (1991), compomers (1996) and lately giomers (2000) appeared on the market.

1.1.1. Natural and synthetic polymeric matrices

Natural polymers have applications in many branches of dentistry: prevention, odontology, endodontics, prosthetics and surgery. For polymeric matrices used especially in bone augmentation, the main features are: biocompatibility, imitation of the three-dimensional structure of hard tissues and physical and mechanical properties as close as possible to those of the tissues they replace. Their resorbability is not negligible, they must be gradually replaced by newly regenerated tissue.

For this purpose, a variety of natural polymers, including extracellular matrix proteins such as collagen, have been used; polysaccharides such as chitosan, alginate, starch and cellulose; as well as glycosaminoglycans, such as hyaluronic acid. Some of the natural polymers can provide a model for the formation of biomimetic apatites, which is highly desirable for inducing fast colonization of the bone. Recent studies conducted by Hutchens et al. have shown the ability to replace bone tissue by cellulose-based composites (Fig.1.1) that contains hydroxyapatite. [3].

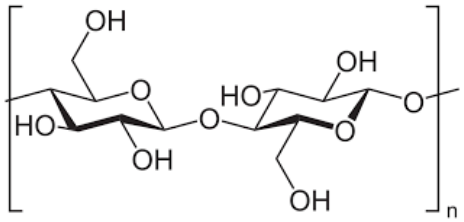

Fig.1.1 *Cellulose structure*

Synthetic polymeric matrices are found in a wide range of composite resins and hybrids developed more recently: compomers, ormocers and giomers. It is known that the composite resins used in dentistry typically contain an organic matrix based on bisphenol A 2,2-bis [4- (2'-hydroxy-3'-methacryloyloxypropoxy) phenyl] glycidyl methacrylate (Bis-GMA) propane), which is the most commonly used monomer since its synthesis by Bowen (1956). [6]

1.1.2. Inorganic fillers

Composite resins contain an inorganic filler incorporated into the polymeric matrix. The proportion of inorganic filler varies between 70-85% depending on the manufacturer, the application range, as well as the fillers composition: glass, silicon, hydroxyapatite, quartz, etc.

The type of particles varies in both shape (round, pearls, fibers) and sizes. The fillers are added into the resin to improve the mechanical resistance, aesthetics and decrease of polymerization shrinkage and thermal expansion coefficient. Also, the inorganic filler in the resins improves the physico-chemical, optical, mechanical properties such as traction, compression, modulus of elasticity, hardness and abrasion resistance.

1.2. Adhesive systems with applications in dentistry

1.2.1. Composition of adhesive systems

The same as composite resins, adhesive systems contain acrylic monomers as the basic component. They form the matrix in which are embedded all the other components: organic solvents, polymerization activation system, inhibitors, and sometimes inorganic fillers.

The polymeric matrix is the one that gives the adhesive the physico-mechanical properties after the polymerization. Two types of monomers are included in the adhesive systems: crosslinking monomers (crosslinkers) and functional monomers. Functional monomers contain a single polymerizable group and a functional group which gives them the characteristics of functional monomers as opposed to cross-linking monomers containing two or more polymerizable groups. By polymerization, the functional monomers form a linear network and the crosslinking monomers lead to the formation of a three-dimensional cross-linked network which provides superior strength and mechanical properties to the adhesive. This is why the crosslinking of monomers is important in order to increase the strength of the adhesive.

1.2.2. Classification of adhesive systems

1.2.2.1 Classification by application steps

If the adhesive system contains 3 components: the etching agent (orthophosphoric acid), the primer (functional monomers) and the adhesive resin (crosslinking monomers), it is applied in three steps.

When the crosslinking and functional monomers are conditioned in the same bottle (etch and rinse system) and when the etching agent is conditioned with the primer in the same bottle and the adhesive resin is conditioned separately (self-etching adhesive system), the adhesive system is applied in two steps.

In the self-etch adhesive system where the etching agent, the primer and the adhesive resin are conditioned in the same bottle, the adhesive system is applied in one step.

1.2.2.2 Classification by adhesion mechanism

The adhesion mechanism to enamel and dentine is in fact a process of replacing the removed minerals from the dental hard tissue with adhesive resin monomers that remain locked after polymerization in the created porosities, which provides an important micromechanical bond. This phenomenon has been called hybridization and has the effect of forming the hybrid layer. The classification of contemporary adhesive systems is based on the adhesion mechanism. Taking this approach into account, three adhesion mechanisms are currently used in modern adhesive systems: etch and rinse adhesive systems, self-etching adhesive systems and adhesives based on glass ionomer cement. [5], [6]

1.3. Giomeri.

1.3.1. History

In the last decades, a new class of hybrid materials, called giomers, was introduced on the international market (2000) by Shofu (Tokyo, Japan). Giomers represents a new concept of adhesive dental biomaterial based on Pre-Reacted Glass Technology (PRG).

1.3.2. Composition, properties and applications

Giomers are a composite material of special structure being composed of an organic matrix and a hybrid filler that contains pre-reacted glass. In giomers, fluoroaluminosilicate glass particles react with the polyacrylic acid, forming pre-reacted glass-ionomers, which are then introduced into the organic resin. Since the acid-base reaction takes place before mixing with the resin, an extended hydrogel layer is formed surrounding the glass particles. This layer participates in the formation of a well-defined matrix in which the fluoride ion release and recharge can be controlled.

As a dental restorative material, the giomers are able to combine the advantages of two large classes of restorative dental material: composite resins and GIC, exhibiting increased optical, mechanical properties, increased radioactivity, clinical stability, composite resin-like handling properties, and at the same the GIC biocompatibility and the fluoride ion release and

recharge properties. Because of these advantages, their indications of use are the most diverse and complex in dentistry practice. [7], [8], [9], [10]

Chapter 2. Smart materials: giomers

The objective of the research was the preparation and characterization of a series of new biomaterials from giomer class. The new experimental giomers were obtained in the form of pastes by dispersing new hybrid fillings into original photopolymerizable resin matrices. Novelty in the composition of experimental giomers consists in the use of polyacid based on acrylic acid, itaconic acid and N-acryloyl leucine P (AA-co-IA-co-LeuM) or P (AA-co-IA- co-Leu) grafted or not with light-curing metacrylic groups, as the main starting component in the synthesis of pre-reacted glasses instead of polyacrylic acid used by Shofu in their giomers formulations.. In addition, another novelty element is the use of a bis-GMA analogue urethane-tetrametacrylic monomer in the resin matrix instead of commercial bis-GMA dimethacrylate monomer used in commercially available giomers. The start hypothesis is that such structures introduced into the organic matrix will lead to a low polymerization shrinkage and a high degree of polymerization of the vinyl groups.

2.1. Experimental models for hybrid fillings used in giomers

Two type of pre-reacted glass (PRG1 and PRG2) were obtained by the conventional method used in the preparation of glass ionomer cements (GIC). PRG1 was prepared by mixing the 50% aqueous solution of polyalkenoic acid P (AA-co-IA-co-Leu) with a superficially active glass powder having the SiO_2 oxide (49%), Al_2O_3 (22%), CaF_2 %) in a weight ratio of 1 / 2.4.

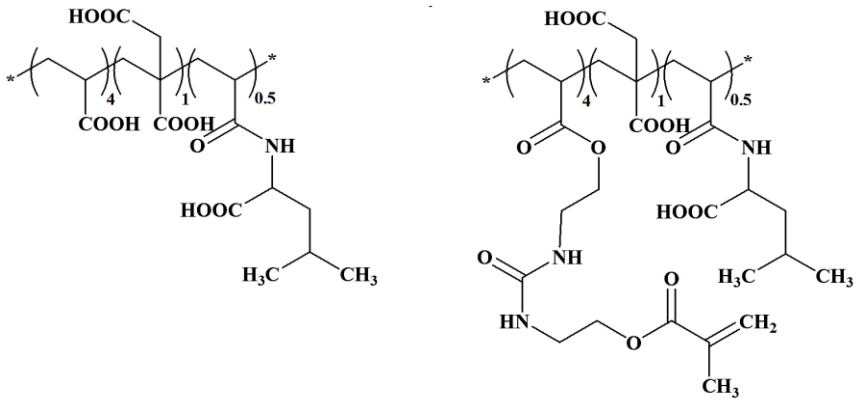

P(AA-co-IA-co-Leu) **P(AA-co-IA-co-LeuM)**

Fig. 2.1. *The modified polyalkenoic acids used in experimental PRG*

After 7 days, the pre-reacted glass PRG1 was dried in the oven at 95 ° C for 24 hours. Finally, PRG1 was grinded in a ball mill and sifted to obtain a fine powder. PRG2 was obtained in a similar manner; with the only difference that the copolymer P (AA-co-IA-co-LeuM) was used instead of polyalkenoic acid P (AA-co-IA-co-Leu). The structure of the modified polyalkenoic acids used in experimental giomers is shown in Figure 2.1.

Based on pre-reacted glass PRG2, radiopaque glass fillers and fluorohydroxyapatite (FHAp), 3 hybrid fillings were prepared in order to use them in the preparation of experimental giomers.

The compositions of the experimental hybrid filler are shown in Table 2.1:

Table 2.1. Compositions of the experimental hybrid filler

Nr. Crt.	Hybrid filler			
	PRG2	FHAp	Radiopaque glass	Al_2O_3
U1	50%		50%	
U2	35%	15%	50%	
U3	30%	10%	50%	10%

2.2. Experimental models for the organic matrix used in giomers

In order to obtain giomers with improved properties, in the resin composition, an Bis-GMA urethane-tetramethacrylate analogue (Bis-GMAexp) was used in addition to commercial Bis-GMA monomer (Bis-GMAcom).

The experimental analogue of Bis-GMA (Bis-GMAexp) was obtained by the addition of methacryloyloxyethyl-2-bromoethylurethane to the commercially available Bis-GMA hydroxyl groups. Triethylene glycol dimethacrylate (TEGDMA) was used as the diluent monomer. The components of the photochemical initiation system, CQ photosensitizer (0.5% by weight), DMAEM accelerator (0.65% by weight) and BHT inhibitor (800 ppm) were dissolved in TEGDMA prior to mixing with Bis-GMA monomer (Bis-GMAcom or Bis-GMAexp).

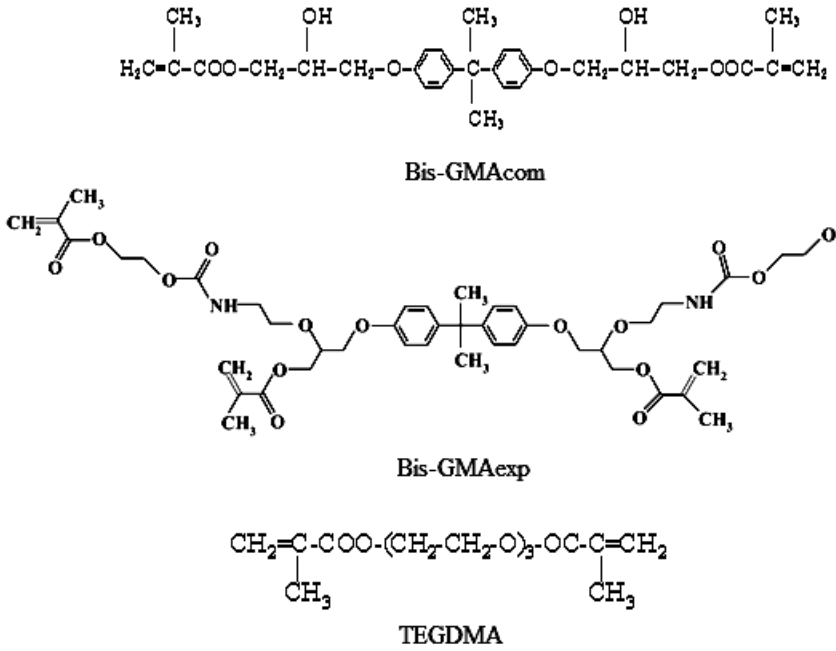

Fig. 2.2 *Structure of monomers used in the organic matrix of experimental giomers*

2.3. Preparation and structural characterization of restorations giomers and pit and fissure sealant giomers

The difference between the restorations and sealants is their viscosity and thus the percentage of filler added to the organic matrix: the powder / liquid ratio is 45/55 in the sealant giomers and 80/20 in the restoration giomers. The consistency of the restorations is dull and is used to restore the tooth following loss of dental tissue. The consistency of the sealants is fluid in order to be able to adapt perfectly to the dental anatomy. They are applied prophylactic to the healthy tooth, on the occlusal face in order to prevent the appearance of caries.

Experimental light cured restoration giomers were prepared as a monopaste by mixing the resin with the hybrid filler U1, U2 and U3 presented in the previous paragraph. The resin matrix consisted of commercial bis-GMA or modified Bis-GMAexp and triethylene glycol dimethacrylate (TEGDMA), respectively. The photochemical initiation system (camphorquinone 0.5% and 1% dimethylaminoethyl methacrylate compared to the monomer mixture) was dissolved in the resin matrix.

The composition of experimental restoration giomers is presented in Table 2.2

Tabel 2.2. The composition of experimental restoration giomers

Nr. Crt.	Organic matrix			Hybrid filler
	Bis-GMAcom	Bis-GMAexp	TEGDMA	Cod
G1	70%		30%	U1
G2	70%		30%	U2
G3	70%		30%	U3
G4		70%	30%	U1
G5		70%	30%	U2

Based on the two components, the organic matrix and the hybrid filling, 4 compositions of pit and fissure sealant material were made in the form of photopolymerizable pastes. Monomer mixtures were prepared from the commercial bis-GMA basic monomer or the original bis-GMAexp urethane dimethacrylic monomer together with the triethylene glycol dimethacrylate diluent (TEGDMA) respectively. The hybrid fillings used included fluorohydroxyapatite, radiopaque glass, and the original pre-reacted glasses PRG1 and PRG2.Table 2.3. presents the compositions of the experimental pit and fissure giomer sealants

Tabel 2.3. The compositions of the experimental pit and fissure giomer sealants

Giomer code	Organic matrix (L)		Hybrid filler (P)		Filler/ resin (P/L)
	Component	%	Component	%	
S11.	Bis-GMA$_{com}$ TEGDMA	60 40	PRG1 FHAp Radiopaque glass	20 20 60	1/1
S12.	Bis-GMA$_{com}$ TEGDMA	60 40	PRG2 FHAp Radiopaque glass	20 20 60	1/1
S21.	Bis-GMAexp TEGDMA	60 40	PRG1 FHAp Radiopaque glass	20 20 60	1/1
S22.	Bis-GMAexp TEGDMA	60 40	PRG2 FHAp Radiopaque glass	20 20 60	1/1

Chapter 3. Testing of new advanced giomer biomaterials

After the preparation of the experimental materials, they were tested to obtain the most advantageous formulations to submit to a clinical trial.

3.1. Determining the degree of conversion

Following the evaluation of the residual double bonds (DLR) and therefore the degree of conversion(GC) of the monomers, the conclusion was that there was a significant difference between the conversion (100% -DLR%) obtained for the experimental giomers containing commercial Bis-GMA and the the experimental giomers containing the original urethane Bis-GMAexp. Thus, in the case of G4 giomer and G5 giomer the conversion is 78.9% and 72.12% respectively, compared to 45.27%, 54.26% and 49% recorded for G1giomer, G2 giomer and G3 giomer, respectively. In conclusion, the giomers prapared with the original Bis-GMA exhibit improved conversions relative to giomers prepared with commercial Bis-GMA

Table 3.1. Residual double bonds and conversion rates for experimental giomers

Cod probă	Abs_I 1637,27 cm^{-1}	Abs_I 1608,34 cm^{-1}	Abs_F 1637,27 cm^{-1}	Abs_F 1608,34 cm^{-1}	DLR %	GC %
G1	0,0552337	0,0436631	0,0523952	0,0756773	54,73	45,27
G2	0,065678	0,0446629	0,0334386	0,0497155	45,74	54,26
G3	0,0700374	0,0504211	0,0460098	0,0649384	51,00	49%
G4	0,0517486	0,0166301	0,00621201	0,00946184	21,10	78,9
G5	0,0561891	0,0181846	0,0239651	0,0278212	27,88	72,12

3.2. Determination of water absorption and solubility

Determination of water absorption was performed in accordance with international standard ISO 4049/2000. In Figure 3.1. water absorption is reported after 1, 2, 3, 6 and 7 days for the 5 experimental giomers.

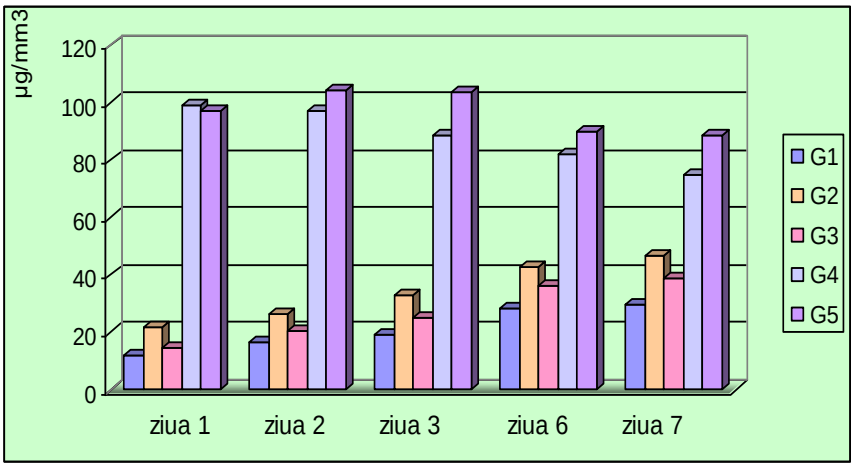

Fig. 3.1. *Water absorption for experimental giomers G1-G5*

From Fig. 3.1 it can be seen that the water absorption values for G1, G2, G3 are much lower than the values for the G4 and G5 giomers. In this case, water absorption is primarily influenced by the nature of the polymeric matrix in the giomers and much less by the nature of the hybrid filler; the high values recorded for the G4 and G5 giomers are due to the hydrophilic urethane polymer matrix in their composition.

The water solubility for giomers containing commercial Bis-GMA was negative: -5.09 µg / mm3 for G1, -2.83 µg / mm3 for G2 and -2.26 µg / mm3 for the case G3. In the case of G4 and G5, the solubility recorded positive values, reaching 10, 12 µg / mm3 in the case of G5.

3.3. Evaluation of coloristic stability

To determine the color differences of the giomers after exposure to colorants, disc-shaped specimens (30 mm diameter x 2 mm thick) were made which were hardened in the same way photoactivated in 17 points on the surface of the specimen. The prepared giomers specimens were maintained for 72 hours in red wine (pH = 2.5), concentrated black coffee (pH = 4.6) and orange juice (pH = 3.8) according to ADA Specification No. 12 and Lee Pharmaceuticals. After storage, the giomers specimens were placed in a Unicam 4 UV-VIS spectrometer. The (a *, b *, L *) coordinates of the reflectance spectrum were recorded, and the color differences ΔE * in the CIELAB system were calculated using the formula below:

$$\Delta E^* = (\Delta L^{*2} + \Delta a^{*2} + \Delta b^{*2})^{1/2}$$

where ΔL * represents the difference in brightness between the two samples

Δa * represents the difference between the "red-green" coordinates corresponding to those two samples

Δb * represents the difference between the corresponding "yellow-blue" coordinates of the two samples

The differences (Δa *, Δb *, ΔL *) were also determined by analyzing the digital images of the final and initial state of the giomer specimens using a specific software ("Discolor").

In Table 3.2. the L *, a *, b * and ΔE * values are presented for the 5 experimental giomers in the initial state (R-Reference) and the final state after keeping in red wine (W), coffee (C) and orange juice respectively

Table 3.2. Color differences of the experimental giomers after exposure to red wine, coffee and orange juice

	G1				G2				G3				G4				G5			
	L	a	b	ΔE	L	a	b	Δ E	L	A	b	ΔE	L	a	B	ΔE	L	a	b	ΔE
R*	79,4	1,1	7,9	-	76,5	1,4	8,6	-	89,5	0,1	5,1	-	81,8	1,24	9,38	-	85,34	1,24	9,6	-
W *	74,5	-0,2	19,2	12,4	76,9	-0,7	17,8	9,4	85,1	-2,3	24,5	20,03	77,4	-0,5	14,74	7,18	80,14	-1,1	16,0	8,6
C *	74,7	1,7	12,6	6,6	77,6	1,06	12,5	4,0	86,2	0,18	10,9	6,65	79,2	0,03	1,11	4,7	81,52	-0,4	14,8	6,6
J*	76,9	1,2	9,52	2,9	76,5	0,08	10,9	2,6	89,1	0,03	6,05	1,05	79,7	0,44	10,68	2,58	82,71	-0,2	9,6	2,15

* - Reference, W * - red wine, C * -coffee, J * orange juice

Color stability was superior in the case of urethane polymer matrices (G4 and G5) that were least colored. These results were obtained by two methods: using reflection spectra and digital image processing respectively by means of a software application (DISCOLOR).

3.4. Determination of bending strength and modulus of elasticity

The bending resistances of the experimental giomers (both based on commercial Bis-GMA and experimental Bis-GMA) are close to the resistance of commercial giomer Beautifil II (100.5 MPa) being 10-12 Mpa lower, instead the modulus of elasticity for experimental materials exceeds the value for commercial material (9.05 GPa). Bending strength values are within the ISO 4049/2000 limits, the lower limit for a composite restorative material being 80 Mpa.

3.5. Determination of the amount of fluoride ions released

In the fluoride ion release test, the results showed after the first storage day values ranging from 0.25 to 0.47 ppm for the experimental giomers compared to 0.07 ppm for commercial giomer (Beautifil II) and after seven days values from 3.52 to 9.26 ppm for the new giomers compared to 2.56 ppm for the commercial giomer. The values obtained for the cumulative fluoride ion release were higher for all experimental giomers than for the Beautifil II product, being twice as high as those obtained for the commercial product, after 60 days storage in water.

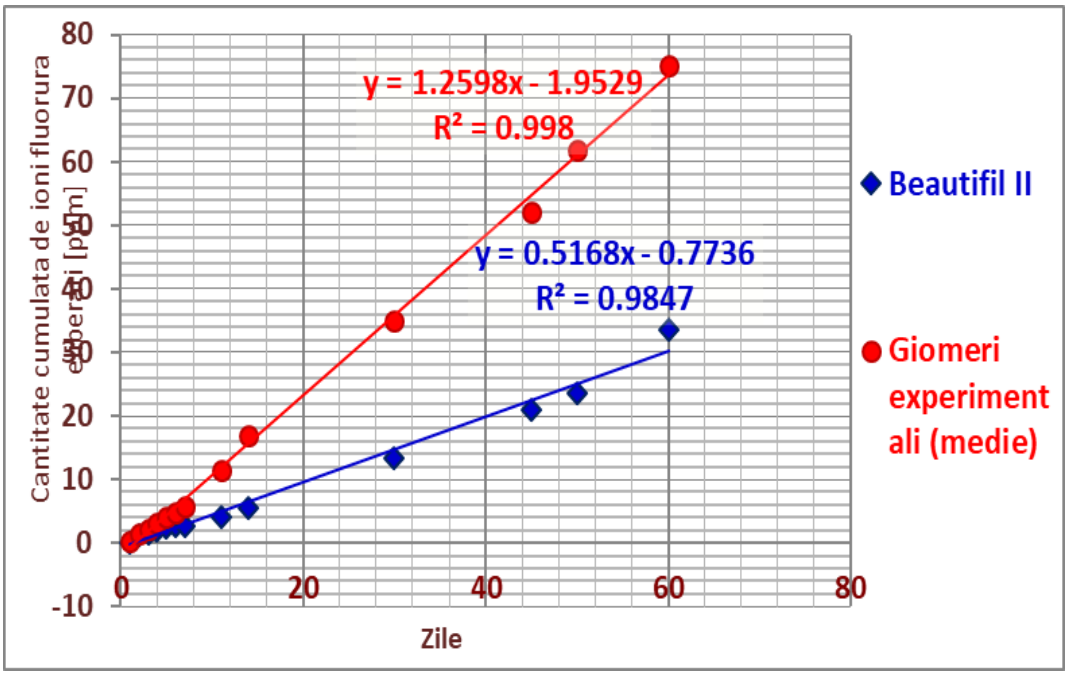

Fig 3.4. The cumulative amount of fluoride ion released over time by the experimental giomers (average) and Beautifil II commercial giomer

The amount of fluoride ion released for all experimental giomers sealants exceeds the amount of fluoride ions released by the commercial product for the same period of time after 50 days of storage in distilled water, this being approximately two times higher for the S11 and S12 giomers, and three times higher for the S21 and S22 giomers than for the Beautifil II product.

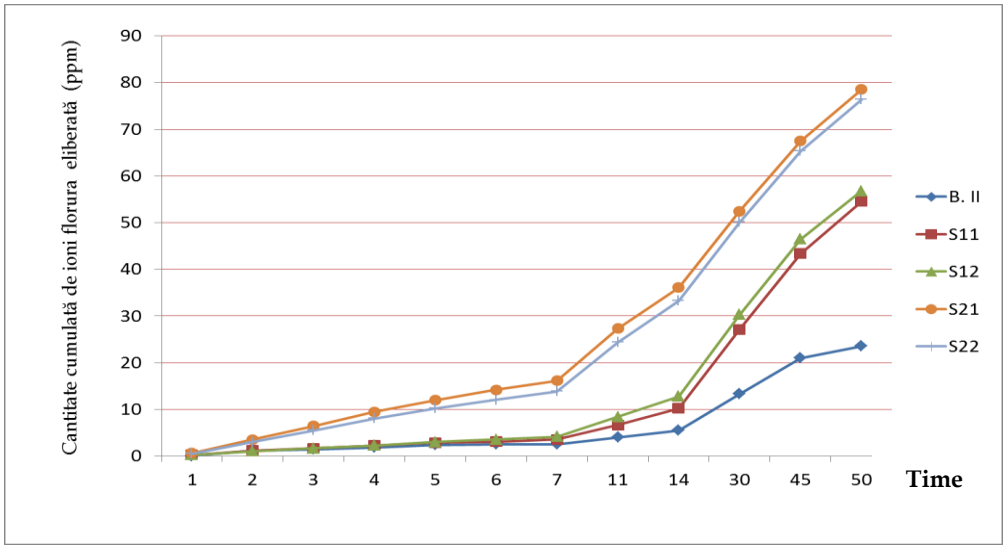

Fig. 3.5. The cumulative amount of fluoride ion released over time by experimental giomers sealants compared to the commercial product Beautifil II

The differences between the S11 and S12 giomers on the one hand and the S21 and S22 giomers on the other hand can be explained by taking into account the chemical nature of the base monomer in the two groups of giomers. The original Bis-GMA$_{exp}$ urethane dimethacrylate present in the composition of the S21 and S22 giomers gives the polymer matrix a pronounced hydrophilic character and a higher permeability for the release of fluoride ions compared to the hydrophobic character and high stiffness of the commercial Bis-GMA monomer. When comparing experimental polymers with the same organic matrix but different pre-reacted glass, it can be seen that materials having PRG1 in composition release constantly a slightly higher amount of fluoride ions.

3.6. Radiopacity evaluation

The radiopacity values of the giomer samples were expressed in equivalent aluminum thickness (mmAl).

Giomer	Beautifil II	G11	G22
Radiopacity [mm Al]	2.99	2.15	2.21

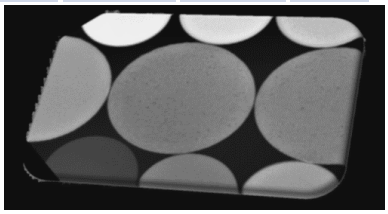

Fig. 3.6 The radiopacity values of the giomer samples G11 şi G22

As can be seen from the following radiographic image (Fig.3.6), all giomers exhibit radiopacity greater than 2mm Al, being above the limit imposed by international standard ISO 4049/2000 (1mm Al). Dental enamel has a radiopacity of 2 mm Al, and dentine, radiopacity of 1 mm Al.

A radiopacity greater than 2mm Al of a material is considered to be very good as it gives the dentist the opportunity to clearly distinguishes the interface between the material and the dental tissue on the radiographic image, thus avoiding possible diagnostic confusions and, consequently, inappropriate treatment.

Chapter 4. Adhesive systems used in combination with giomers

4.1. Preparation and characterization of new dental adhesive systems

In this study, two two-steps innovative adhesive systems (A1 and A2) containing a primer and an adhesive resin were prepared and investigated. The two adhesive systems are different by different primers, the adhesive resin being the same in both systems. Primers 1 and 2 (from A1 and A2, respectively,) were prepared starting from modified polyalkenoic acids (PAIk-1MA and PAIk-2-MA, respectively). Palk-1MA is the acrylic acid / itaconic acid copolymer modified with methacrylic groups. Palk-2-MA is the copolymer of acrylic acid / itaconic acid / N-acryloyl leucine modified with photopolymerizable groups. The polyalkenoic acid formulas used in the primers 1 and 2 are shown in the figure 4.1

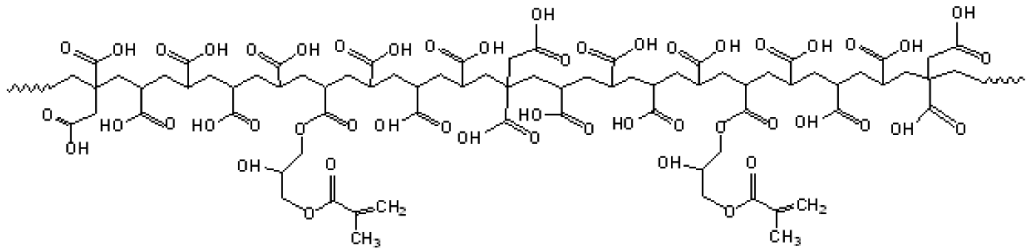

PAIk-1-MA

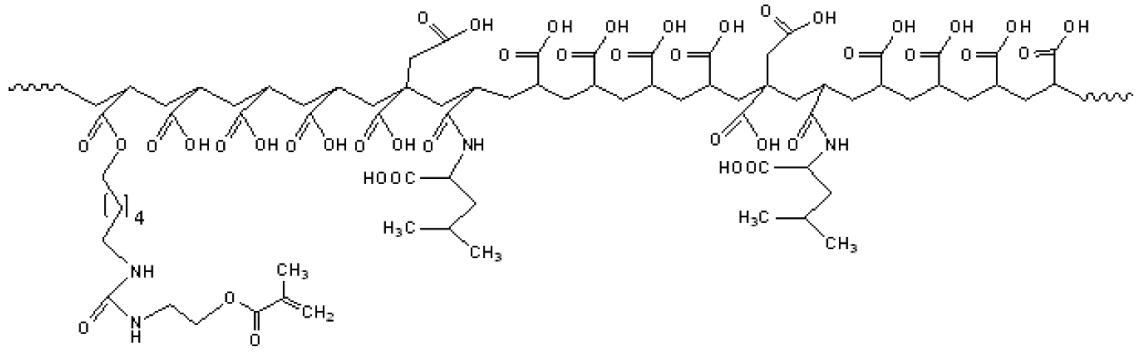

PAIk-2-MA

Fig.4.1 The modified polyalkenoic acids used for the obtaining of the primers

The experimental giomer based on commercial bis-GMA and PRG2 was selected, after evaluating the physico-chemical properties of the experimental giomers, to be further tested for adhesion and adaptation to the cavity walls with the two experimental adhesive systems.

4.2. Evaluation of adhesion

The evaluation of microleakage at the tooth / restoration interface was assessed by the penetration of colored liquids method and also by lock-in thermography, a new non-destructive method of investigation. The interface morphology was examined by scanning electron microscopy techniques (SEM) and atomic force microscopy (AFM) techniques. The commercial giomer Beautifil II and its adhesive system FL-Bond II were used for comparison. The commercial adhesive system used as a reference FL-Bond II, is a two-step self-etch adhesion system consisting of a primer and a bonding FL-Bond II primer contains adhesion promoter monomer an acetone or HEMA-free .

The composition of the investigated adhesive systems is presented in Table 4.1.

Table 4.1

Composition of the adhesive systems investigated in the study

Code	Composition of the adhesive systems				
	Main components	**Diluting monomers**	**Photo-Initiation system**	**Solvents**	**Filler**
Primer 1	PAlk-1-MA (30%)	HEMA (32%) TEGDMA (10.7%)	CQ (0.18%) CDFI (1.12%)	H_2O (20%) Acetone (6%)	-
Primer 2	PAlk-2-MA (30%)				
Primer FL-Bond II Shofu, Kyoto, Japan	4-AET 6-MHPA	-	photo-initiator	H_2O Ethanol	-
Bonding	Bis-GMA (60%)	HEMA (20%) TEGDMA (18.53%)	CQ (0.49%) DMAEMA (0.98%)	-	-
Bonding FL-Bond II Shofu, Kyoto, Japan	UDMA	HEMA TEGDMA	photo-initiator	-	S-PRG

PAlk-1-MA, Poly(acrylic acid-co-itaconic acid) modified with methacrylic groups; PAlk-2-MA, Poly(acrylic acid-co-itaconic acid-co-N-acryloyl-L-leucine) modified with methacrylic groups; 4-AET, 4- acryloxyethyltrimellitic acid; 6-MHPA, 6-methacryloxyhexyl phosphonoacetate; Bis-GMA, 2,2-bis[4-(2-hydroxy-3-methacryloxy-propoxy)phenyl]propane; UDMA, 1,6-bis(methacryloxy-2-ethoxy-carbonylamino)-2,4,4-trimethylhexane; HEMA, 2-hydroxyethyl methacrylate; TEGDMA, triethyleneglycol dimethacrylate; CQ, camphorquinone; CDFI, diphenyliodonium chloride; DMAEMA, N,N-dimethylaminoethyl methacrylate; S-PRG, surface pre-reacted glass.
Abbreviations: %: percentage by weight.

4.2.1. Marginal infiltration method

The most widely used microinfiltration test method described in the literature is the dye penetration method after thermocycling the samples for 500 cycles that simulates the aging of dental restorations by heat stress similar to that produced in the oral cavity. This method is a non-destructive method which is based on the technique of liquid penetration in cracks and surface defects. It involves the preparation and the restoration of cavities on teeth, the isolation of the external surface of teeth except 1 mm around the restoration and then submerge the teeth in dye for 24 hours [11] . The evaluation of this infiltration is performed on tooth slices crossing the restoration by assesing scores according to the depth of dye infiltration according to a standardized ISO protocol [12]

A schematic view of the microleakage ISO scoring system is shown in Fig. 4.2.

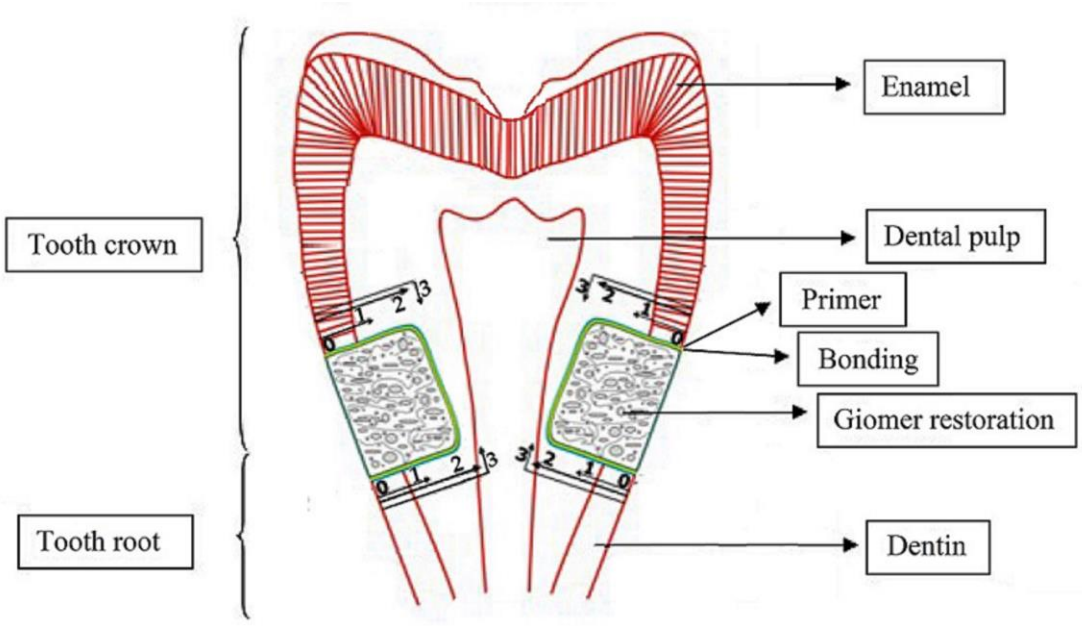

Fig. 4.2. Longitudinal tooth slice through the giomer restauration showing the microleakage scoring system;

0 - no dye penetration;

1 - dye penetration till ½ length of the wall;

2 - dye penetration to the full depth of the cavity wall, but not including the axial wall;

3 - penetration reaches the axial wall

4.2.2. Electronic Scanning Microscopy (SEM)

The Electronic Scannig Microscopy (SEM) method can be used successfully in the morphological investigation of textures, contours and geometric forms of microparticles in various fields.

With SEM analysis, images can be viewed at high magnification (50x-10000x and over). In this technique, the surface of the sample is scanned by an electron beam to produce a variety of signals depending on many factors, including the electron beam energy and the nature of the sample, the response being collected by a detector, as described by Saghiri et al. [13]. SEM is used to analyze or measure voids that are formed between the restorative material and the dentine or enamel wall, thus performing the adhesion interface analysis. [14]

4.2.3. Atomic Force Microscopy (AFM)

Atomic Force Microscopy (AFM) is a non-destructive technique of surface analysis that, unlike other types of microscopy, builds a map of the heights of the examined surface. The AFM is mainly used to obtain sample's topography. Without damaging it, it is possible to visualize the three-dimensional structure of the surface under consideration. Investigation of the sample is done by means of a needle called cantilever and the investigation can be done depending on the contact of the cantilever with the sample: in contact mode, noncontact and semicontact mode or intermittent contact. This mode is chosen according to the properties and characteristics of the sample. The generated AFM image can be viewed from any angle and the dimensions of the irregularities (width, height, depth, diameter) can be assessed.

4.2.4 Thermocalorimetric method of adhesion assessment (lock-in thermography)

The inconveniences of current techniques have led to the development of a new methodology for automatic detection of defects localized at the tooth-restoration interface by lock-in thermography and complex imaging algorithms. This method gives us the benefit of a complete dental restoration assessment through a non-invasive technique, infrared radiometry having excellent potential for use in various branches of the medical field. In this method, an

intensity-modulated excitation source (light) is sent to the sample to be investigated, generating a modulating temperature field at the absorption site. This modulated thermal field, issued by the sample, can be measured with an infrared detector. The major problem is that the tooth has a non-homogeneous structure consisting of four types of tissue arranged in layers: enamel, dentin, cement, dental pulp (Figure 4.3), each layer having its own inhomogeneities and thermal and optical properties. [15]

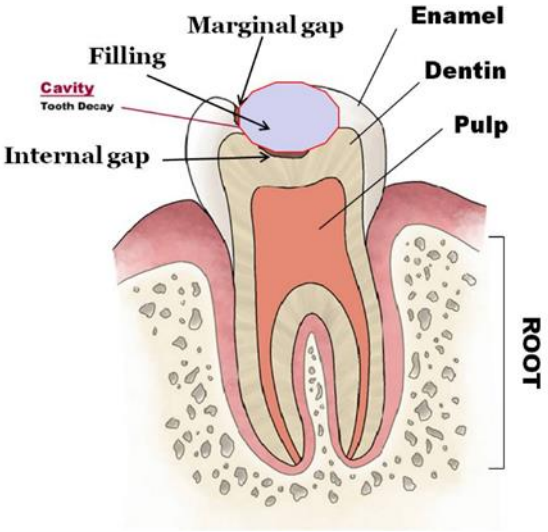

Scattering of light into the tooth is high, because the tooth is a very heterogeneous environment. For example, due to the presence of dentinal tubulis and organic components, light diffusion is greater in dentine than enamel, which is relatively translucent.

Figure 4.3: *Structure of a tooth with a restored cavity*

At the same time, the amount of light scattered is a key factor in determining the depth of light penetration into tissue. A photothermal signal is generated only when thermal energy is released following a photon absorption event in the analyzed tissue. Therefore, in order to obtain an optimal photothermic response (signal), the wavelength of the excitation source must be carefully chosen, taking into account both the scattering coefficients and the light absorption coefficients in enamel and dentin. For these reasons, heat generation and heat transfer in diffuse environments such as the tooth is a complicated physics problem in which the phenomena of photon scattering and absorption in each layer of the tooth have to be taken into account at the same time.

Thermography is a non-contact technique in which an IR (infrared) camera captures the infrared radiation emitted by a surface and displays them in a color map, each color corresponding to a particular temperature. IR thermography is used either by simply observing isotherms on the surface of interest (passive approach) or by stimulating the external thermal response (active approach) in order to obtain a good thermal contrast between the area of interest and the background.

In dentistry, IR thermography is mainly used to monitor the polymerization temperature of dental composites during the polymerization process. [16], [17]. There are only two recent publications (2013) in which the interface between the restoration material and the tooth was evaluated by lock-in thermography (LIT) [18], [19]

4.3. Comparative study of the performance of adhesive systems

Evaluation of microleakage

The dye penetration score and the percentage of the dye penetration length were determined on 42 tooth slices, with one slice being selected from each tooth. The slice where the dye penetration was the most intense was selected to represent the tooth.

The two restorations on each of the selected slices were investigated using an Olympus KC301 inverted microscope (Olympus America, Center Valley, PA, USA) at 40x magnification. The dye penetration length along the tooth-restoration interface was recorded in μm using QuickPhoto Micro 2.2 software (Olympus). The staining along both enamel and dentin walls was scored using the ISO microleakage scoring system [12].

Percentages of dye penetration length were calculated using the formula presented below:

$$\text{Percentage of dye penetration length} = \frac{\text{Length of the stained interface}}{\text{Total length of the interface}} \times 100 \qquad (1)$$

Evaluation of interface morphology

Representative slices presenting different microleakage scores were selected from each group to evaluate the interface morphology.

SEM analyses were performed using a Quanta 3D FEG D9399 (FEI, Hillsboro, OR, USA) scanning electron microscope. Samples were prepared by placing the tooth slices onto carbon tape and coating with 10 nm gold evaporated in an argon atmosphere (Sputter Coater Agar) prior to analysis. The thin gold coating was sputtered in three sputtering cycles taking approximately 10 s each.

The AFM investigation of the selected tooth slices surfaces was performed using a scanning probe microscope (JEOL, JSPM 4210, Tokyo, Japan). The microscope was operated in the intermittent contact, also known as tapping mode. The cantilever used had a triangular shape and a silicon nitride tip (NSC11, MicroMasch, Sofia, Bulgaria). The cantilever resonant frequency ranged from 260 to 330 kHz, and the spring constant was approximately 48 N/m. Both a low scanning rate of 1 Hz and a higher rate in the range of 2-6 Hz were used for optimal imaging. All AFM experiments were carried out under ambient laboratory temperature conditions (approximately 20°C). AFM observations were repeated on the following different scanning areas on the sample surface (i.e., for different magnifications): 20 x 20 μm^2 to 10 x 10 μm^2. AFM images were obtained from at least five macroscopic zones separately identified on each sample. All images were processed according to the standard AFM procedure. The surface topography, phase and amplitude were simultaneously recorded.

The experimental IR setup used has been described previous in the literature [20]. It included a heat source, a waveform generator, an IR camera and a computer for data acquisition (figure 4.4). The intensity-modulated optical stimulation (f_0 = 0.2 Hz) was delivered by a frequency-doubled Nd : YAG laser (Laser Quantum OPUS with λ = 532 nm and tunable power, with 0.5 W maximum power). Considering the thermal diffusivities $\alpha_{dentine}$ =26 × 10^{-4} cm^2 s^{-1} and α_{enamel} = 42 × 10^{-4} cm^2 s^{-1} [21],[22], the thermal diffusion lengths at this frequency are about 600 µm in dentine and 800 µm in enamel. In order to be detected, the crack must be located within the heat diffusion region. The laser spot was focused at filling–enamel or filling–dentine interfaces, at an appropriate distance from the boundary. The IR camera (FLIR 7200 series, with a 256 × 320 pixel array of InSb detectors sensitive in the 1.5–5.1 µm wavelength range) recorded the changes in the surface temperature of the specimens at a frame rate of 100 images s^{-1}. The signals delivered by the IR camera and the reference signal were sent to the lock-in detection module, which records pixel by pixel the IR signal and calculates the amplitude and

the phase of its modulated component at the frequency f_0, as well as the continuous image. The optical axis of the camera was perpendicular to the investigated surface. By using a macro lens (G1 type) with a working distance of 300 mm, a spatial resolution of 30 µm is achieved. The average laser power (set at 50 mW) was measured by means of a 400–1100 nm selectable wavelength laser powermeter. In order to increase the signal-to-noise ratio, the IR signal was averaged over 50 excitation periods.

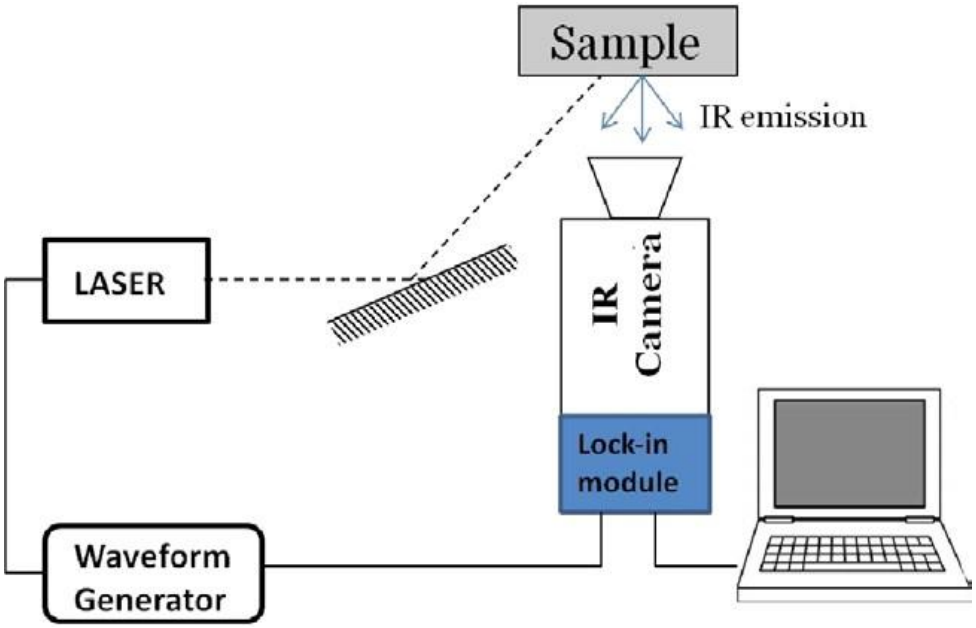

Figure 4.4. Lock-in thermography experimental setup

Statistical analysis

Data were statistically analysed via one-way analysis of variance (ANOVA) using the SPSS (IBM Statistics Desktop, V22.0) software package. Tukey's test with the level of significance set at 0.05 was used to determine the presence of statistically significant differences between the mean values of the percentage of dye penetration length of the tested materials.

The microleakage behaviour examined using the scoring method is presented in Table 4.2, and the percentage of dye penetration length measured along the dentin/adhesive and enamel/adhesive interfaces is shown in Table 4.3

Table 3

Microleakage scores measured in dentin and in enamel

Materials (Group)		Microleakage scores							
		Dentin				Enamel			
		0	**1**	**2**	**3**	**0**	**1**	**2**	**3**
Number (%) of resto-rations made with different materials	FL-Bond II / Beautifil II (control) (Group I)	8 (29)	6 (21)	4 (14)	10 (36)	28 (100)	0 (0)	0 (0)	0 (0)
	A1 adhesive system / giomer G (Group II)	0 (0)	0 (0)	4 (15)	24 (85)	24 (85)	4 (15)	0 (0)	0 (0)
	A2 adhesive system / giomer G (Group III)	2 (7)	12 (43)	14 (50)	0 (0)	28 (100)	0 (0)	0 (0)	0 (0)

.

Table 4

Percentage of dye penetration length along the tooth-restoration interface
Mean values (N=28) and (standard deviation)

Materials (Group)	**Percentage of dye penetration length (%)**	
	Dentin	**Enamel**
FL-Bond II/ Beautifil II (control) (Group I)	23.32 (21.01)[a]	0.00 (0.00)[a]
A1 adhesive system / giomer G (Group II)	58.15 (18.68)[a b]	1.82 (2.54)[a b]
A2 adhesive system / giomer G (Group III)	14.74 (8.43)[b]	0.00 (0.00)[b]

Note: Superscript letters within columns indicate mean values statistically significant different from each other, when compared using the Tukey test, $P < 0.05$.

Table 4.2 shows that the microleakage scores in the enamel area were 0 in all investigated samples except for 4 restorations belonging to group II (A1 and giomer G).

At the dentin margins, the investigated samples restored with FL-Bond II and Beautifil II (control, group I) showed all scores in the range (0, 1, 2 and 3), whereas in the samples restored with the A2 adhesive system and giomer G (group III), the only scores found were 0, 1 and 2, with the highest microleakage score of 3 being absent. Scores 2 and 3 were found in group II, showing that notable microleakage was present in all of the samples restored with the A1 adhesive system and giomer G.

In Fig. 4.5, representative optical microscopy images of tooth slices showing different microleakage scores in the enamel and dentine margins are provided.

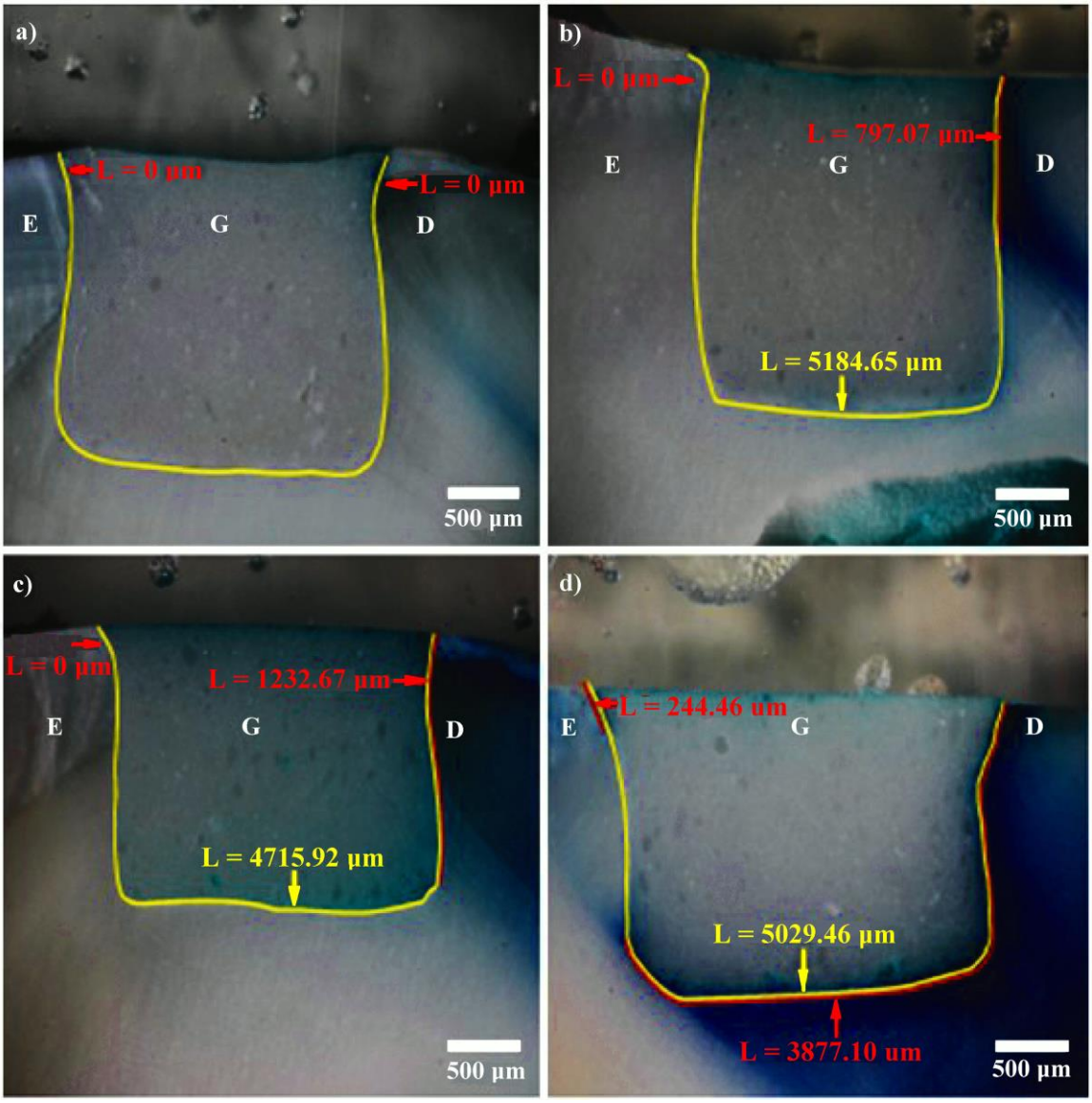

Fig. 3. Optical microscopy images of tooth slices presenting different microleakage scores at enamel (E) and dentin (D) margins: a) 0 (E) and 0 (D) - group I; b) 0 (E) and 1(D) - group I c) 0 (E) and 2 (D) - group III; d) 1(E) and 3 (D) - group II.

Yellow trace- cavity perimeter (total length of the interface)

Red trace- colorant infiltration (length of the stained interface)

The results from Table 4.3 showing the percentages of dye penetration length at the dentin margin as well as at the enamel margin were consistent with the results obtained for the microleakage scores (Table 4.2). The percentages of dye penetration length at the dentin margin obtained in the restorations made using the A1 adhesive system and giomer G (group II) were 2.5-fold higher than those obtained for the restorations made using FL-Bond II and Beautifil II (Control) and almost four-fold higher than those for the restorations made using the A2 adhesive system and giomer G (group III). The percentages of dye penetration length at the dentin margin obtained for the restorations made using the A2 adhesive system and giomer G (group III) were 1.5 times smaller than those obtained for the restorations made using FL-Bond II and Beautifil II (Control).

Statistical analysis indicated significant differences in the percentages of dye penetration length at the enamel margin ($p=4.626\times10^{-6}$) and at the dentin margin ($p=3.701\times10^{-15}$), as determined by one-way ANOVA.

Tukey's post-hoc test revealed that there was a statistically significant difference between group I (control) and group II as well as between group II and group III at both the dentin and enamel margins. At the dentin margin, similar significant differences were observed when comparing group II with group III ($p=5.100\times10^{-9}$) and when comparing group I with group II ($p=5.191\times10^{-9}$). The same pattern occurred at the enamel margin, showing similar significant differences between the groups. Comparisons of group I with group II and group II with group III revealed significant mean differences at the 0.05 level ($p=3.918\times10^{-5}$).

The differences between group I and group III were not statistically significant at the dentin margin ($p=0.148$) or the enamel margin ($p=1.000$).

The differences in the microleakage scores observed in the enamel compared to the scores obtained in the dentin could be explained by the morphological differences in the tooth structures dentin and enamel. The enamel structure is based on hydroxyapatite (Hap) crystals at 92% vol., 2% vol. organic materials and 6% vol. water [23]. Its structure allows the creation of microretentions by etching of the surface. This process will ensure a perfect interlocking with the components from adhesives, leading to the realisation of a perfect adhesion at the interface. In contrast, dentin is more hydrophilic, with a canalicular structure consisting of 48% vol. Hap,

29% vol. organic materials and 23% vol. water [23]. The dentinal tubules traverse the entire dentine, oriented from the dentin-enamel junction towards the dental pulp. Even if the dentin is dried before the adhesive system is applied, dentinal fluid reappears, almost constantly endangering the adhesion [24]. This structure of the dentin makes it more vulnerable to microleakage than enamel [25-28].

The twofold mechanism of adhesion to dentin is relatively similar for the experimental adhesives and for the commercial one ("mild" self-etch approach), the adhesion being realised by micromechanical interlocking and chemical interactions [6]. When an experimental primer (PAlk-1-MA or PAlk-2-MA) was applied on the dentin, the polyalkenoic acid dissolved the smear layer, partially demineralized the dentin and form strong ionic bonds with the calcium from the hydroxyapatite [29,30]. The demineralization of dentin was minimal in this case because the hydroxyapatite buffered the weak polyalkenoic acid [28]. A zone of chemical interaction (inter-diffusion zone, ion-exchange layer) with a thickness of a few micrometers was formed in which the calcium polyalkenoate salt can hardly be dissolved [6]. After applying the bonding and the visible light, due to the grafted methacrylic groups, the polyalkenoic acids were able to polymerise with the TEGDMA and HEMA from the primer and with the monomers from the bonding, leading to the formation of a unique polymeric network of the adhesive.

When the "mild" self-etch FL Bond II primer was applied, the infiltration of acidic monomers and the partially demineralization of dentin occurred, creating the micro-porosities for micro-mechanical interlocking [31]. A shallow hybrid layer is formed by the infiltration of the monomers in the hydroxyapatite-coated collagen fibril network. Additional chemical interactions between the acidic monomers (4-AET and 6-MHPA) and calcium ions from residual hydroxyapatite occurred [32]. However it is possible that 4-AET calcium salt (Ca-4AET) to have a relatively high solubility as the calcium salt of 4-methacryloyloxyethyl trimellitic acid (Ca-4MET) has, being therefore not very stable [33].

The differences concerning microleakage between the experimental groups (II and III) could be explained by taking into consideration the chemical composition of the primers. The two adhesive systems (A1, A2) contained two different primers (primer 1 and primer 2) in which the main components were polyalkenoic acids modified with polymerisable groups (PAlk-1-MA and PAlk-2-MA, respectively) and a bonding agent based on Bis-GMA. The polyalkenoic acid

with pendant amino acid moieties (PAlk-2-MA) presented more flexibility, allowing more freedom and less steric hindrance when the carboxylic groups interacted with the calcium ions from the dental hydroxyapatite [31], [33]. As a consequence, more carboxylic groups interacted with the calcium ions from the dental tissues in the case of PAlk-2-MA from primer 2 compared to PAlk-1-MA in primer 1. In addition, because PAlk-1-MA exhibited a degree of functionalisation of carboxyl groups with methacrylic moieties approximately 10-fold greater than that of PAlk-2-MA (20% versus 2.5%), the number of free carboxyl groups that could interact with Ca2+ of dental hydroxyapatite was much higher for PAlk-2-MA. This behaviour led to improved sealing and adhesion when using PAlk-2-MA (primer 2). Finally, PAlk-2-MA contained L-leucine residue, respective pendant (-CO-NH-) amide groups which can lead to the formation of additional hydrogen bonds with the carboxyl groups of collagen [33].

SEM and AFM used next to investigate the interface, are powerful tools for the surface investigation of various sample types (e.g., nanoparticles, bio nanocomposites, biomaterials) [34-36], [21]. Tapping-mode AFM investigation was performed to characterise the tooth-restoration interface by revealing its topography.

Fig. 4.6 a and 4.6 b show SEM photomicrographs of the dentin surface treated with the A2 adhesive system and restored with giomer G. Fig. 4.6 c and 4.6d present SEM photomicrographs of the interface between dentin, FL Bond II adhesive and Beautifill II giomer.

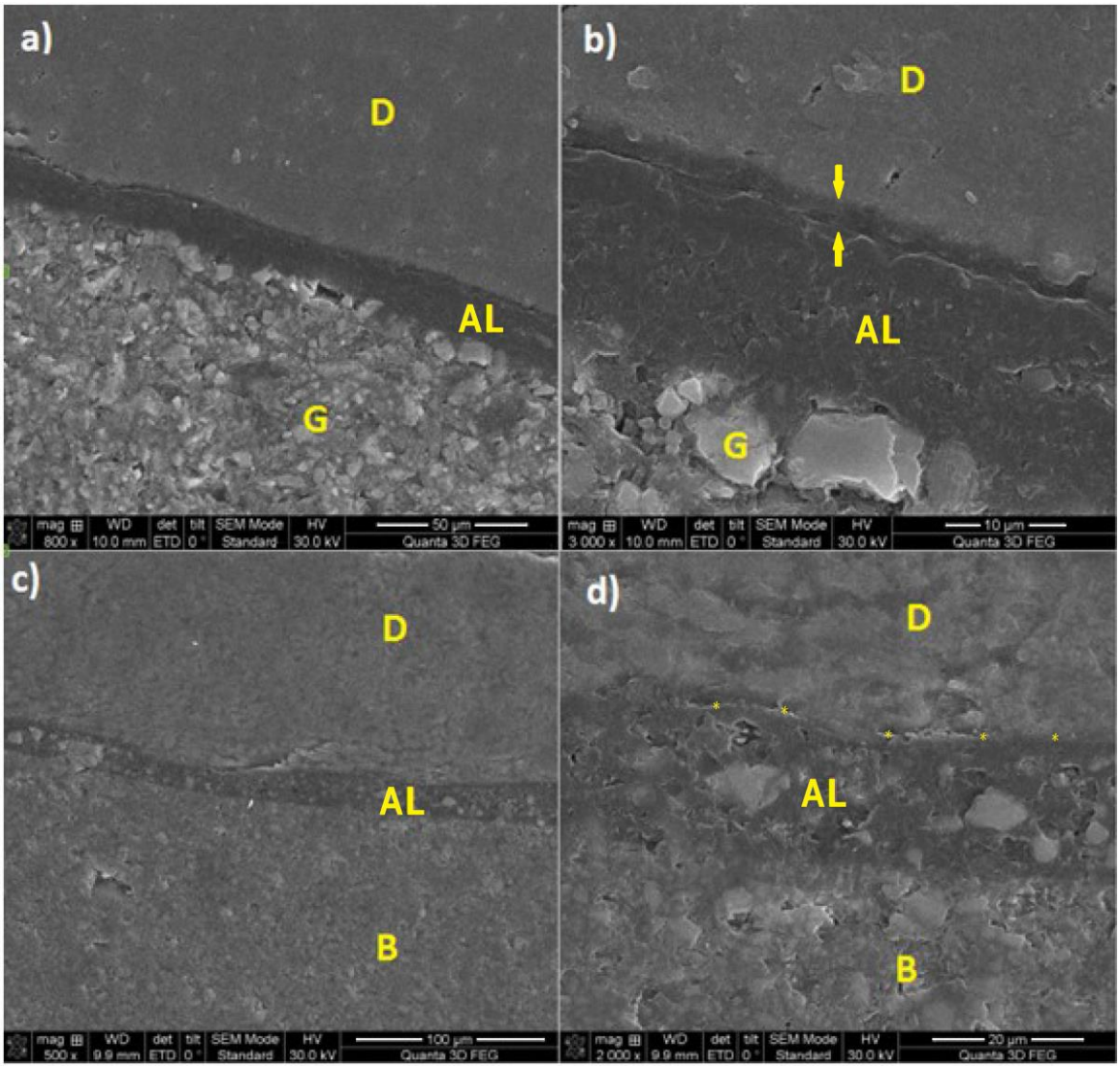

Fig. 4.6 SEM photomicrographs of the interfaces: a), b) dentin / A2 adhesive / Giomer G ; c, d) dentin / FL Bond II / Beautifil II. Arrows show the margins of the ion-exchange layer. Asterisks show the adhesion interface to dentin.

(D) - dentin; (AL) – adhesive layer ; (B) - Beautifil II; (G) - Giomer G

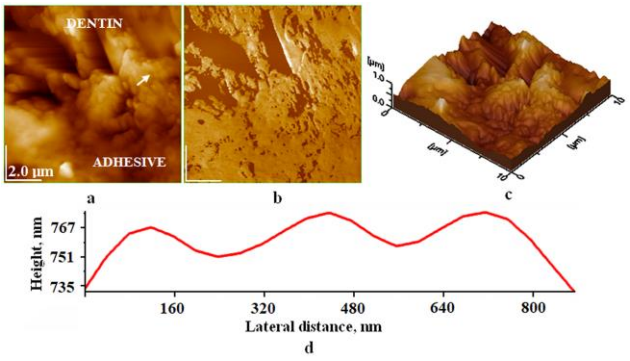

Fig. 4.7. AFM images obtained at adhesion interface between dentin / A2 adhesive / Giomer G: a) topographic image, b) phase image, c) 3D – view of image (a), and d) cross section on white arrow in figure (a). Scanned area 10 µm x 10µm.

In Fig.4.7 the AFM images at the adhesion interfaces between dentin/A2 adhesive/giomer G are shown.

In Fig. 4.6a and 4.6 b, the good sealing ability of the A2 adhesive system to the dentin substrates and to giomer G can be observed. The dentin presents a smooth surface punctuated by small dots representing the dentin tubules. The microstructure detail in Fig. 4.6 b reveals the adhesion interface with dentin at a higher resolution. The ion-exchange layer ranged from 1 to 2 µm. The adhesive layer with a thickness of about 10 µm can be observed between the ion-exchange layer and giomer G. Giomer G has a more heterogeneous microstructure based on a granular matter having polyhedral shape. A large amount of particles measuring less than 10 microns with sharp or rounded edges as well as a few particles having a diameter of about 20 microns can be visualized in Fig. 4.6 b. Base on the particle size analysis, the first can be attributed to the radiopaque filler particles or small sizes SPRGexp particles and the second ones can be attributed to the large sizes SPRGexp filler particles[37]

The adhesion interface (hybrid layer) between the dentin and Beautifil II appears as an undulated layer closely following the shape of the dentin and having approximately the same width along the interface (Fig. 4.6 c, 4.6 d). The adhesive layer thickness ranged from 18 to 20 µm, and the SPRG filler particles showed irregular polyhedral shapes varying in size from 5 to15 µm. The morphology of the adhesion zone is better observed at higher magnification in Fig. 4.6d.

A good connection was established between the adhesive and the giomer restoration. The surface morphology of Beautifil II shows particles of various sizes, mostly below 15 microns having irregular shapes, too. One can observe a greater amount of particles embedded in the polymer matrix than in the experimental giomer. The black pores on the samples surface in the SEM images of the giomers appeared due to the preparation of the samples (sectioning and sanding) during which particles of different sizes can be detached from the polymer matrix.

The adhesion morphology of the interface between dentine / adhesive A2 /Giomer G is observed in AFM images, Figure 4.7, at high magnification. The dentin is situated at the top of the topographic image in Figure 4.7a and the adhesive is situated at the lower side of the image. The ion-exchange layer formed by the reaction between polyalkenoic acid and dentin hydroxyapatite has a thickness of about 2 μm. The topography of this layer reveals its nanostructure which contains of nano-particles having the average diameter around 80 nm, as observed in the cross section in Figure 4.7d. These nano-structural units can be attributed to the reacted hydroxyapatite with the polyalkenoic acid. A good sealing of dentinal tubule is observed and an optimal cohesion between dentin and adhesive is achieved. The fact is sustained by phase image, Figure 4.7b, where dentin, ion-exchange layer and adhesive appears as a single solid block having light brown nuance meanwhile dentinal tubule is featured in dark brown. The three-dimensional view of topographic image, figure 4.7c, presents the bonding achieved by A2 adhesive in a more suggestive manner. The ion-exchange layer in good cohesion with the dentin is better observed.

The SEM and AFM images are in close agreement with the results obtained by the dye penetration method, showing that the A2 adhesive system provides effective sealing of the giomer G restorations to the tooth substrate without gaps or voids.

The lock-in thermography investigation method was used to complete the information on the adhesion interface at the selected samples.

This method is exemplified below on a tooth slice belonging to group III, restoration performed with Giomer G and the experimental adhesive system A2.

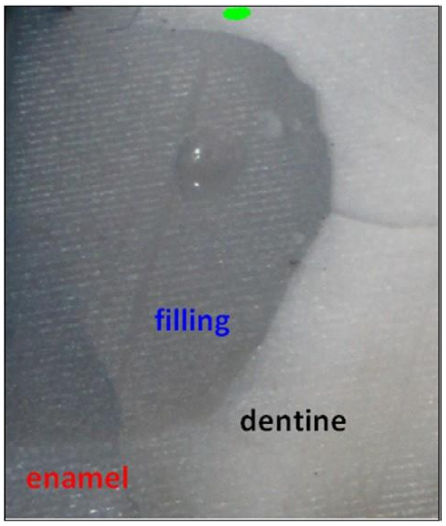

In fig. 4.8 shows the optical image of a slice, belonging to group III (restoration performed with Giomer G and the experimental adhesive system A2) after dye penetration testing. No trace of dye at the tooth–restoration interface is detected, which indicates a good marginal adaptation

Fig.4.8. *the optical image of a slice of tooth (restoration performed with Giomer G and the experimental adhesive system A2)*

The images obtained by lock-in thermography are displayed in figures 4.9(*a*)–(*f*). The position of the heat source is indicated in figure 4.8 by the spot located close to the dentine–filling interface.

Figures 4.9 (*a*) and (*b*) represent the dc image and the profile along the marked line, which are quite disturbed. As the dentine presents numerous dentinal tubules, the laser beam is scattered in the dentine tissue and the excitation spot is expanded on the surface. When light reaches the interface between dentine and filling, it is partially refracted, reflected, and scattered. Depending on the optical properties of the filling and dentine, light can be absorbed preferentially on one side of the interface, providing an additional localized source of heating. An increased IR signal is observed near the edge of the tooth compared to the excitation region (see figure 4.9(*a*)).

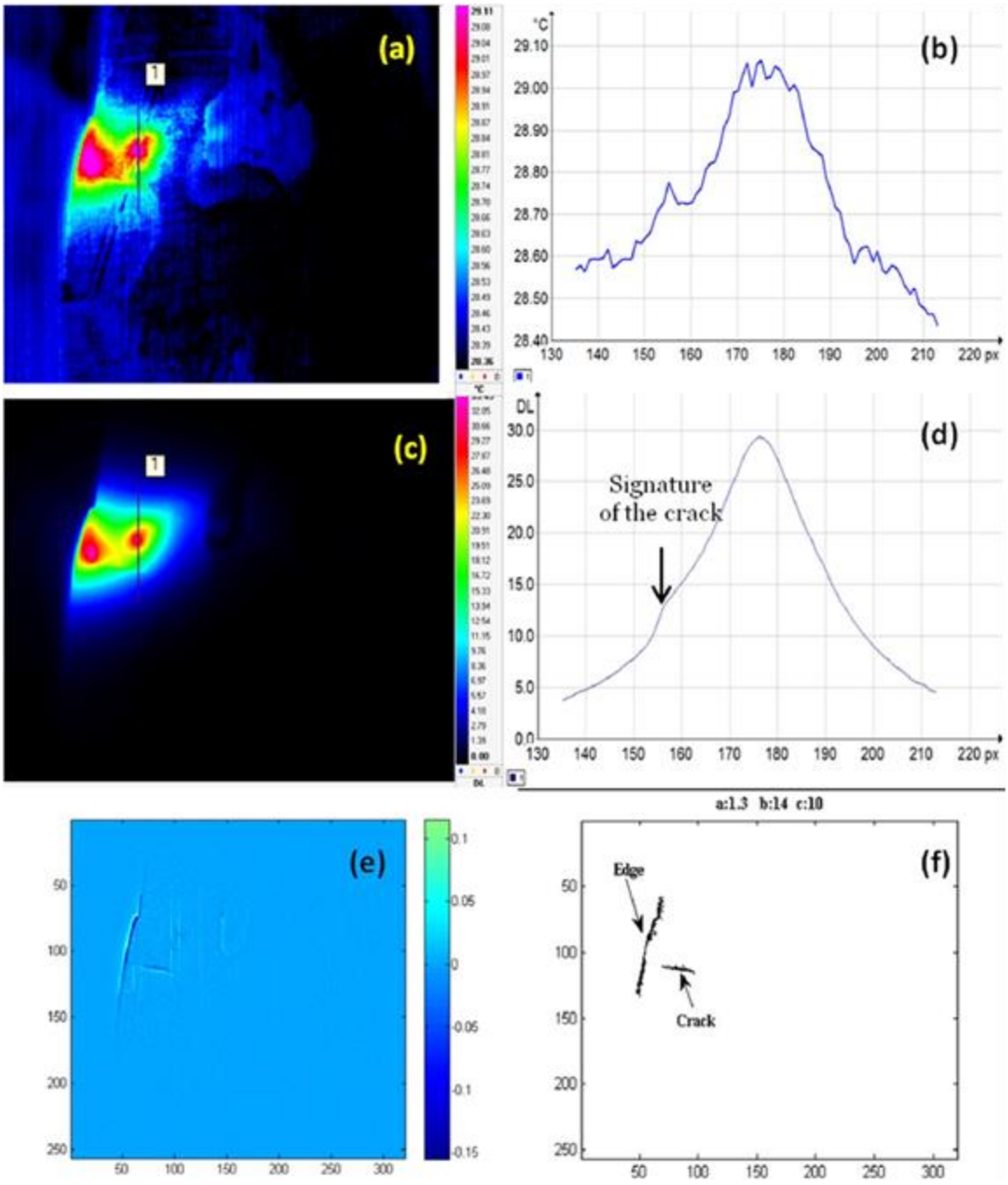

Fig.4.9 *(a) DC image of specimen 2. (b) Profile of the dc image along the marked line. (c) Amplitude image. (d) Profile of the amplitude image along the marked line. (e) $M_b(x, y)$ image. (f) Resulting binary image*.

The amplitude image with the corresponding profile along the marked line is shown in figures 4.9(*c*) and (*d*). The disturbance of the thermal wave due to the presence of a discontinuity is visible at coordinate x = 158. The resulting $M_b(x, y)$ and binary images after applying the

image processing algorithm described in section 2 are shown in figures 4.9(*e*) and (*f*). A failure is detected at the filling–dentine interface, close to the excited area. The length of the detected crack is about 700 μm (23 pixels).

Of the two innovative adhesive systems (A1 and A2) developed for dental restorations to repair enamel or dentin caries by using appropriate clinical protocols, adhesion system A2 based on PAlk-2-MA modified polyalchenoic acid proved a better sealing at the interface with dentine and a perfect adhesion to enamel in dental restorations with giomer. Our findings suggest that microleakage in giomer restorations can be reduced by using a two-step resin-based glassionomer adhesive system containing a polyalchenoic acid with a relatively high molecular weight and specific chemical formula which includes L- leucine and photopolymerizable methacrylic groups. The results described above show that the composition of the adhesive systems influences the sealing, adhesion and binding of giomer restoration to the tooth.

The dye penetration test only detects a gap or fissure at the restoration margins, and the SEM and AFM can be only used ex vivo, being invasive methods of investigation in dental medicine. Lock-in thermography has the most promising results, particularly due to its potential to function in vivo (its non-invasive character) and its ability to detect both marginal and internal defects localized in dental cavities restored with various materials. Thermographic inspection can be done within minutes. This study, carried out on ex vivo transverse teeth sections through giomer restorations, demonstrates the presence of photometric contrast in presence of gaps. Using the second derivative of the amplitude and image processing algorithms improves the quality of the resulting images, increasing the signature of gaps on the surface. The proposed procedure leads to the diagnosis of gaps at the interface having widths of about 1 μm.

4.4. Comparative study of the performance of seal seals

Two light-cured experimental giomers sealants S12, S22 were prepared by mixing in ratio 1: 1 hybrid filling in a resin matrix (Chapter 2). The Fissurit F Vocco GmbH (FS) pits and fissure sealant was used as a control. Ten carious-free teeth (extracted for orthodontic or periodontal purposes) were sealed on the occlusal surface with each material (S11, S12, FS). They were then embedded in acrylate and sectioned longitudinally in slices of approximately 2

mm using a microtome with a diamond disk (Isomet 1000, Buehler, USA) as exemplified in fig. 4.10

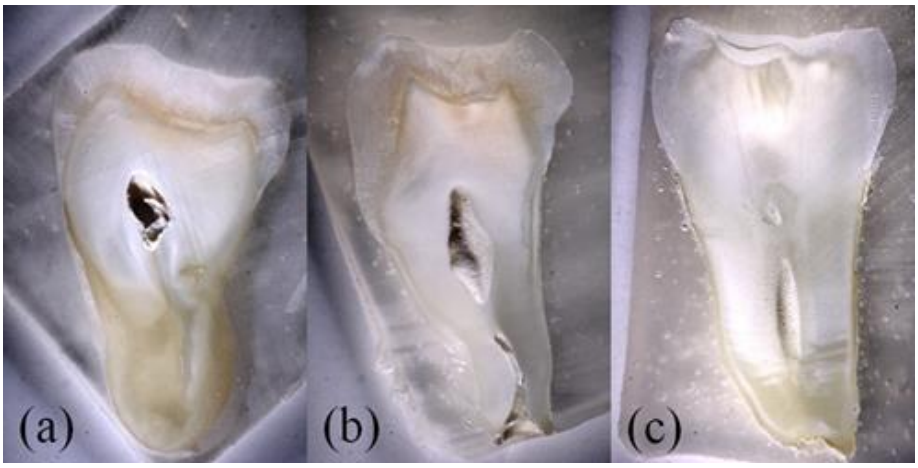

Fig. 4.10. *Slices of teeth sealed with G1 (a), G2 (b) and Fissurit FS (c) and embedded in PMMA.*

The teeth slices belonging to each group were examined by optical microscope, SEM and lock-in thermography. Scanning electron microscopy determinations were performed on an INSPECT S microscope, (FEI Co).

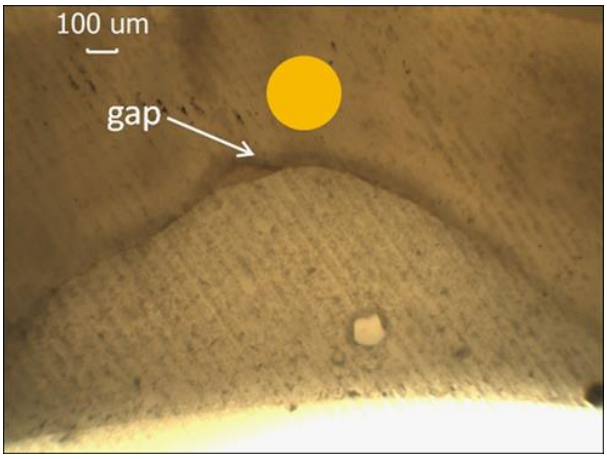

Fig.4.11. *Optical image of sample S22*

An optical image of sample S22 is shown in Figure 4.11. The presence of a gap at the sealant/enamel interface can be observed. The same lock-in procedure was applied to this specimen (the heat source is drawn in Fig. 4.11 by the spot located close to the interface under investigation). In this case the heat flow is disturbed at sealant/enamel interface, as can be clearly seen in amplitude and phase images (see Figs. 4.12 and 4.13).

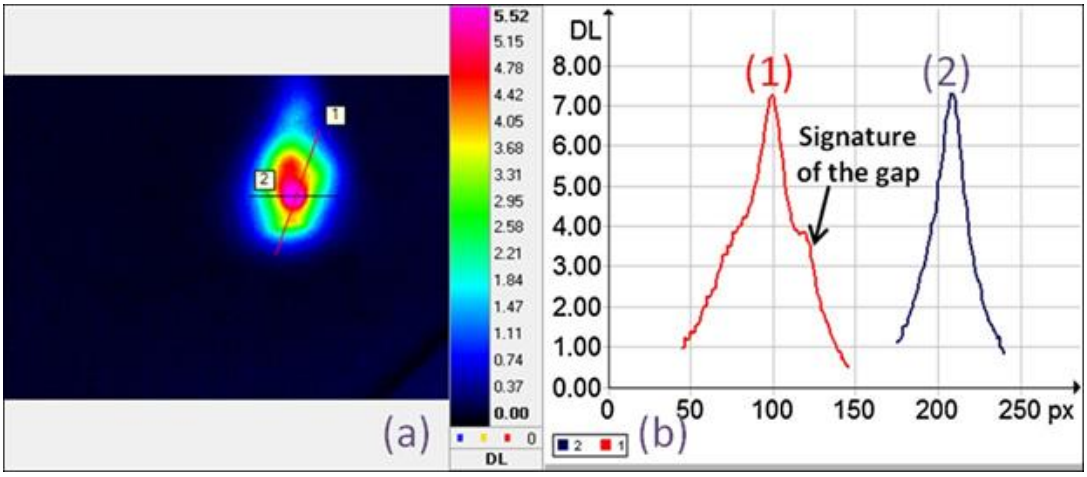

Fig. 4.12. *Amplitude image (a) and corresponding profiles (b).*

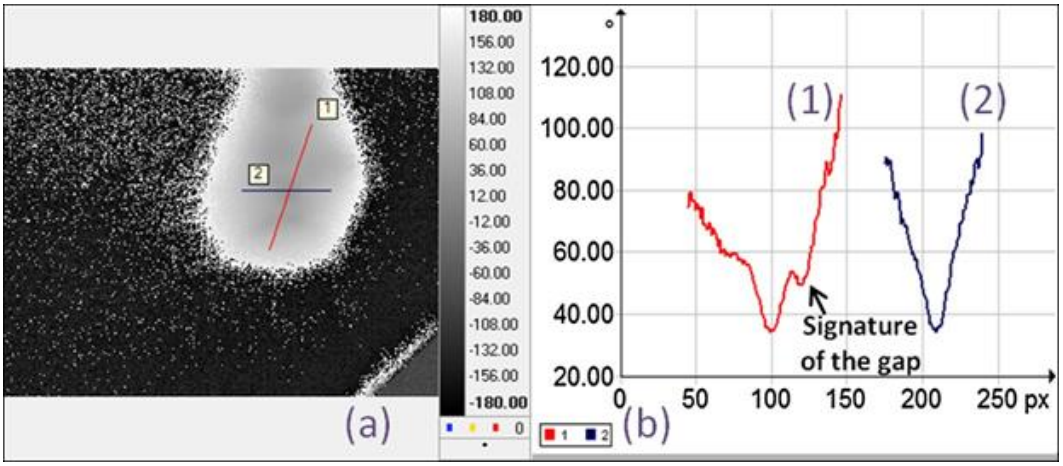

Fig.4.13 . *Phase image (a) and corresponding profiles (b).*

Both amplitude and phase images provide information about the fissure localization on the surface. The thermal wave disturbance above the flaw shows a propagation delay as compared to a reference signal (see Fig. 4.13b) or a small perturbation of the amplitude above the defective zone as compared to sound enamel (see Fig. 4.12b). The gap acts as a thermal barrier disrupting the heat diffusion. To be detected, the gap must be located within the diffusion region of the heat.

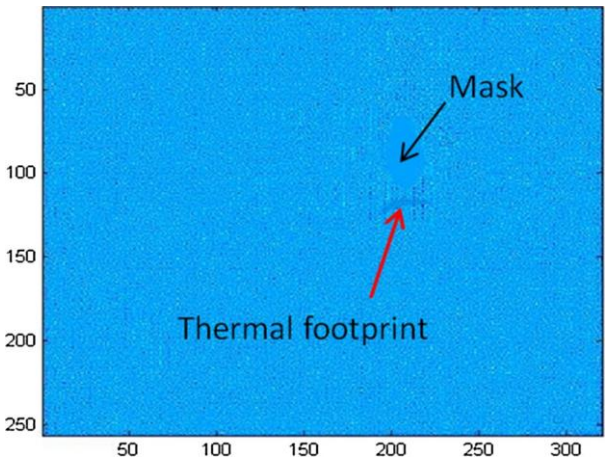

As can be seen in Figs. 4.12 and 4.13, the disruption of the thermal wave is higher in the phase image than in the amplitude image. In order to highlight the small temperature variations surrounding the flow, the second spatial derivative of the amplitude image is applied. In doing so, the contrast given by the presence of a gap at interface is enhanced and more features become visible. The irrelevant fluctuations from the laser area were filtered out, by using a mask. The contour of the gap is only slightly visible, as can be seen in Fig. 4.14.

Nevertheless, by applying the image processing algorithm previously described [38], the binary image showing the signature of the small gap on the surface can't be generated with enough accuracy.

Fig. 4.14 *Enhanced amplitude image.*

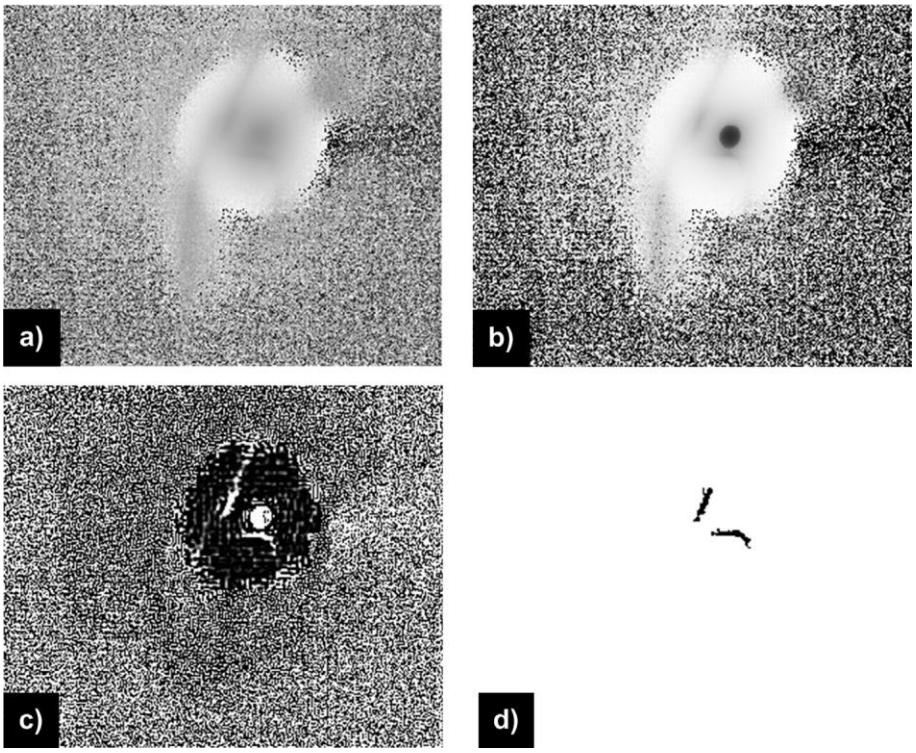

Fig. 4.15. Phase image (a), enhanced phase image I^T (b), Laplacian of the enhanced phase r^2I^T (c), and the resulting binary image (d).

In order to improve the results, we apply the second image processing algorithm on the phase image (Fig. 4.15a). The enhanced phase image I^T is shown in Fig. 4.15b, and the Laplacian of the enhanced phase r^2I^T in Fig4.15c.

The resulting binary image (Fig. 4.15d) clearly reveals the presence of a microgap with a length of 50 μm, located at the sealant/enamel interface. A small fracture in the enamel structure can also be detected (see the slanted line in Fig. 4.15d).

Chapter 5. Material Biocompatibility Assessment

Biocompatibility is one of the most important properties of dental materials and in this chapter we described methods of biocompatibility investigation applied next on the experimental giomer type materials.

5.1. Methods for assessing biocompatibility-in vitro

For the determination of in vitro biocompatibility, the recommended test methods include: direct cell culture and cell culture extract assays; Agar diffusion test; filter diffusion test and dental barrier testing. There is an increasing number (nearly 20) of cell culture techniques in the literature. [39]

5.2 Method of assessment of biocompatibility-in vivo

According to the EUROTOX, CEE, FDA and MS 949/1991 norms for dental restorations materials used in dentistry, it is opted forassesing the tolerance to product implantation tests

The implantation test for these products can be practiced on a laboratory animal species, rats, in two ways: subcutaneous implantation and intramuscular implantation.

All selected animals must be healthy, physiologically normal and must be provided with standard maintenance and nutrition conditions throughout the experiment.

5.3 Evaluation of cytotoxicity and biocompatibility of giomers

The biocompatibility of the experimental restoration giomer G selected for its previously tested properties was tested being named from now on (A1) and the sealant S12 previously selected from the prepared experimental giomer sealant (noted S). Two restoration giomers containing HEMA were prepared: one with HEMA and Bis-GMA and another with HEMA and UDMA. Their composition is presented in Table 5.1.

Table 5.1 Composition of the giomers tested in this study

Giomer	Composition of the giomers			
	Base monomer	**Diluting monomers**	**Photo-Initiation system**	**Filler**
Giomer S	Bis-GMA (32.82%)	TEGDMA (21.89%)	CQ (0.1%) DMAEMA (0.19%)	SPRGexp (9%) F-HA (9%) Barium fluoro-alumino-boro-silicate glass (27%)
Giomer A1	Bis-GMA (13.82%)	TEGDMA (5.89%)	CQ (0.1%) DMAEMA (0.19%)	$SPRG_{exp}$ (28%) F-HA (12%) Barium fluoro-alumino-boro-silicate glass (40%)
Giomer A2	Bis-GMA (13.82%)	HEMA (5.89%)	CQ (0.1%) DMAEMA (0.19%)	SPRGexp (28%) F-HA (12%) Barium fluoro-alumino-boro-silicate glass (40%)
Giomer A3	UDMA (13.82%)	HEMA (5.89%)	CQ (0.1%) DMAEMA (0.19%)	SPRGexp (28%) F-HA (12%) Barium fluoro-alumino-boro-silicate glass (40%)
Giomer	Bis-GMA (7.5%)	TEGDMA (<5%)	DL-Camphorq	SPRG commercial Aluminofluoro-borosilicate

Beautifil II*			uinone	glass (70%) Al2O3

*Material Safety Data Sheet, Beautifil II,http://www.net32.com/images/prodinfo/a/shofu-dental-corp-beautifil-ii-compule-tips-b1-20-pk-1759.pdf

Abbreviations: %: percentage by weight;

Biological assay

Cell cultures: Human dermal fibroblasts HDFa (Invitrogen, Willow Creek, USA USA) and human umbilical endothelial vein cultures HUVEC (Promocell, Hamburg, Germany) were used. Fibroblasts were cultured in Dulbecco's modified Eagle's medium (DMEM) while HUVEC's were cultivated in RPMI medium, both supplemented with 5% fetal calf serum, 50 µg/ml gentamicin and 5 ng/ml amphotericin (Biochrom Ag, Berlin, Germany).

Biomaterial extracts were obtained in compliance with the ISO 10993-12:2012 proceedings. A thin sample (0.5-1mm) of each material ≈3cm2 surface area was incubated, completely submerged in 1ml of culture medium for 24 and 72 hours at 37° C. Six samples were incubated for each giomer composition. The extracts were immediately used for cell viability assays.

Cytotoxicity assay: The cells seeded at a density of 104/well in ELISA 96 wells micro titration flat bottom plaques (TPP, Switzerland) were allowed to settle for 24 hours. Cells were exposed for 24 hours directly to extracts of each biomaterial sample, (prepared as above at 2.11.2) diluted in a range of 1-0.001 in cell culture medium. Cells were then washed and viability was measured by colorimetric measurement of formazan, a coloured compound generated by viable cells using CellTiter 96® AQueous Non-Radioactive Cell Proliferation Assay (Promega Corporation, Madison, USA).

Untreated cultures exposed to medium were used as controls. Briefly, cells were exposed to 20 µl of 3-(4,5-dimethylthiazol-2-yl)-5-(3-carboxymethoxyphenyl)-2-(4-sulfophenyl)-2H-tetra-zolium, inner salt (MTS) /phenazine metosulphate (PMS) mixture (2ml:100µl) in 100 µl fresh

medium/well, for 2 hours, then the optical density values were tested at absorbance of 490 nm by an ELISA plate reader (Tecan, Switzerland). Results are presented as OD490

Statistical method

The statistical significance of the difference in cell viability between the commercial material Beautifil II and the experimental materials was evaluated by 1 tail, paired Student TTEST, using GraphPad; results were considered significant for $p \leq 0.05$ (level of significance $\alpha=0.05$). Statistical package Prism version 4.00 for Windows, GraphPad Software, San Diego, California, USA, www.graphpad.com was used for data analyses.The statistical significance of the difference in cytotoxicity between treated and control groups was also evaluated using the same procedure.

Preparation of specimens for implantation

The *in vivo* testing was done in agreement with the guidelines of the Ethics Committee of "Iuliu Hatieganu" Uiversity of Medicine and Pharmacy, Cluj-Napoca. Sample preparation and implantation tests was done according to(ISO 10993) [40]. From bulk material were moulded sticks having the diameter 1.5 mm and the length 5 mm with round edges that were photopolymerized 40 sec using light cured 'Spectrum 800' (Dentsply, Germany) (470 nm wavelength). After material setting the samples were finished and polished using Super Snap finishing and polishing system (Shofu, Japan) without altering their consistence or hardness. The samples were prepared using Beautifil II and experimental giomers :S and A1 in order to be implanted subcutaneous (dorsal subcutaneous tissue) and intramuscular (gluteal muscle) in 15 wister rats specimens (5per group) under anesthesia. After 30 days the rats were euthanized, following the guidelines of the Ethics Committee, with an overdose of anesthesia (ISO 10993) and the sample were analyzed macroscopic and microscopically and the response was evaluated. The implant site was shaved and the tissues samples from the implant area were carefully excised and transferred to 10% formalin for 5 days fixation process and then embedded in paraffin. Histological sections were then cut at 4 μm and stained with hematoxylin-eosin. The section the most representative was evaluated. Microscopically were assessed the number and type of inflammatory cells found, the presence of new blood vessels, edema, necrosis and the presence or absence of a fibrous capsule (evaluate the repair process). The inflammation at the

implant site was quantify assessing scores[41] depending on the criteria mentioned above and according to the ISO-10993 standards:[40] ISO-10993,

0- Absent: no sign of inflammation

1- Mild :1-5 inflammatory cells of each type/ high powered field (hpf)[×400] ,minimal capillary proliferation (1-3 buds), no edema, early developed capsule

2- Moderate :5-10 inflammatory cells of each type/hpf[×400], groups of 4-7 capillaries with supporting fibroblastic structures, mild edema, partially formed capsule

3- Severe: heavy or packed inflammatory infiltrate, >20 cells/hpf[×400], broad band of capillaries with supporting structures, severe edema, completely formed capsule.

The score given for each criteria were sum up and the results show the biocompatibility of each material tested:

-Non-irritant (0 up to 2.9)

- Slight irritant (3 to 8.9)

- Moderate irritant (9 to 15)

- Severe irritant (over 15)

Cell cytotoxicity:in vitro

All biomaterials tested exerted a decrease in cell viability in a dose related manner, in both cell lines tested (fig.5.1). This effect was also influenced by the preparation time of the extract, mainly with undiluted extracts. The experimental biomaterials showed similar and/or better results when compared to the commercial one, this effect was maintained in all tested conditions (fig. 5.1).

When the undiluted extract was used, cell viability was decreased by all biomaterials when compared to controls. The overall viability of the fibroblasts (fig. 5.1.a,b) was more affected compared to that of the HUVEC's (fig. 5.1. c,d). This could be explained by the fact that fibroblasts are adult cells, with reduced proliferative and regenerative capacities, which

makes them more suitable for biomaterials testing[42], [43] HUVEC's, which are fetal cells, showed better results.

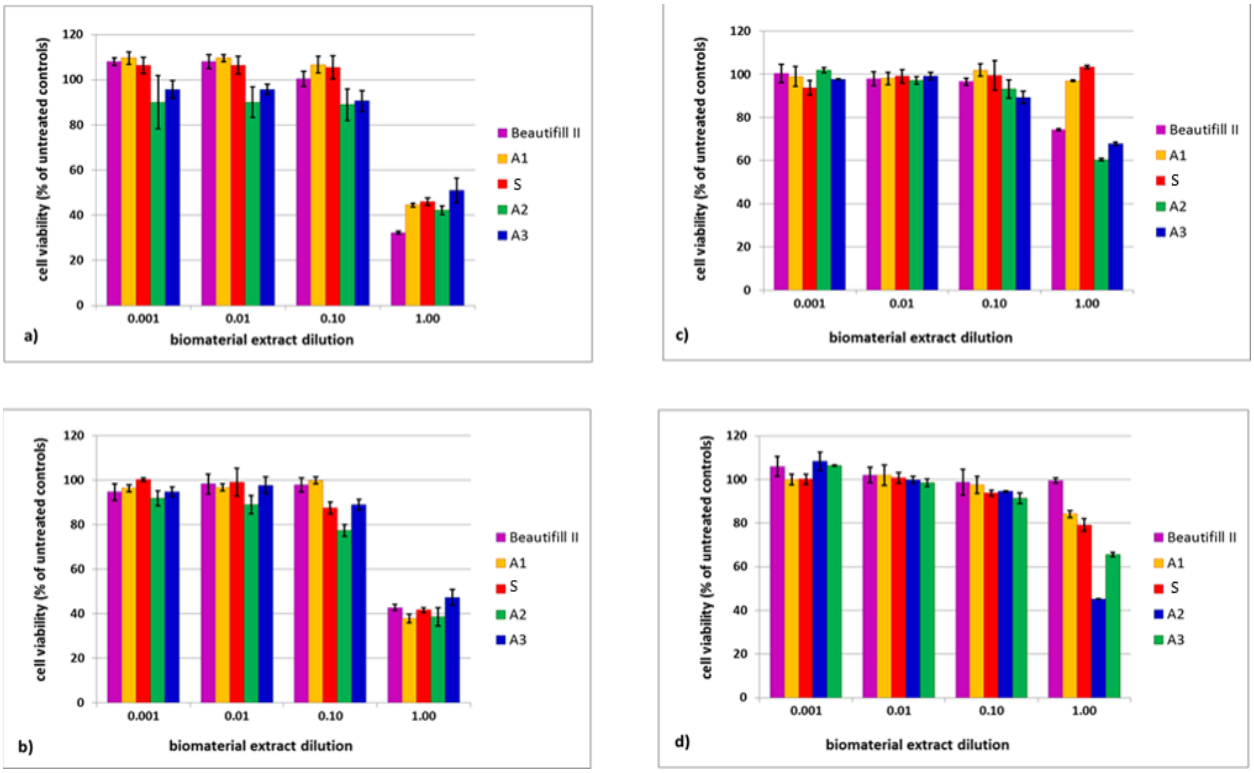

Fig.5.1 *Comparative viability of fibroblasts after 24 hours (a) and after 72 hours (b) giomer extracts exposure and of HUVEC after 24 hours (c) and after 72 hours (d) giomer extracts exposure, respectively*

For statistical analysis, the OD_{490} of each experimental group, for the respective time point, was compared with the untreated control. Cells exposed to the commercial material, Beautifil II exhibited a stronger decrease after 24 hours ($p \leq 3.73E-10$), than 72 hours ($p < 3.57E-09$ for fibroblasts, $p= 3.31E-01$ for HUVEC) compared to controls.

The experimental materials exerted a different effect. They induced a more important decrease following 72 hours ($p \leq 2.62E-07$ for fibroblasts and $p \leq 7.79E-05$ for HUVEC) than for 24

hours (p ≤4.73E-06 for fibroblasts and p ≤ 3.74E-05 for HUVEC, however, p=1.1E-01, not significant for A1) compared to controls.

This is probably due to the physicochemical properties of the compounds which allowed a quicker elimination of the toxic substances in medium when the commercial material was used, but needed a longer contact time for the experimental materials.

As an overview, the less toxic biomaterials on the two normal cell lines tested were S and A1, while the A2 and A3 showed similar results to the commercial product, Beautifil II

Implantation tests: in vivo

After the implantation no changes occurred in the general status or behavior of the rats, both type of implants: subcutaneous and intramuscular were well tolerated, the implantation wound healed without any complication.

The inflammatory infiltrate was observed in both groups in the tissue surrounding the implant, but no necrosis occurred

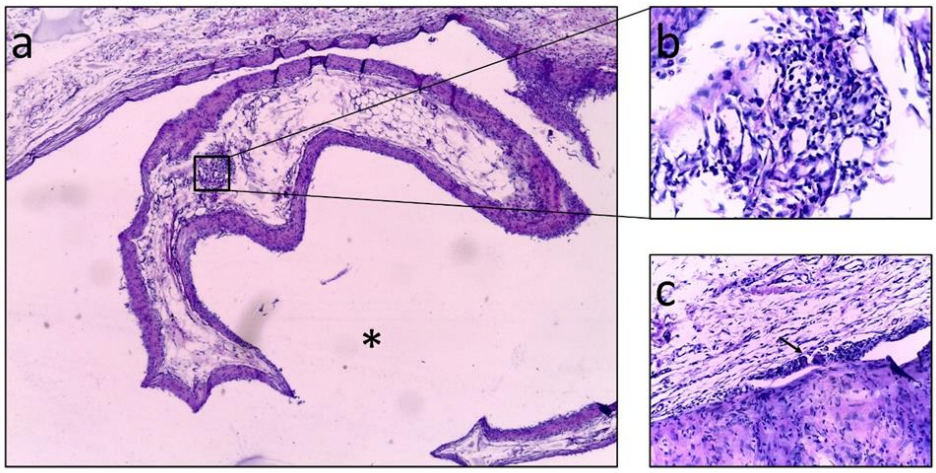

Fig.3 Subcutaneous implant with A1 giomer

* - The place where the implant was

A – 4x Magnification – overview -fybroconjunctive capsule organisation founded in the vicinity of the implant

B – 40x Magnification –- inflammatory infiltrate Lympho- plasmocitary

C –20x Magnification – giant multinuclear cells

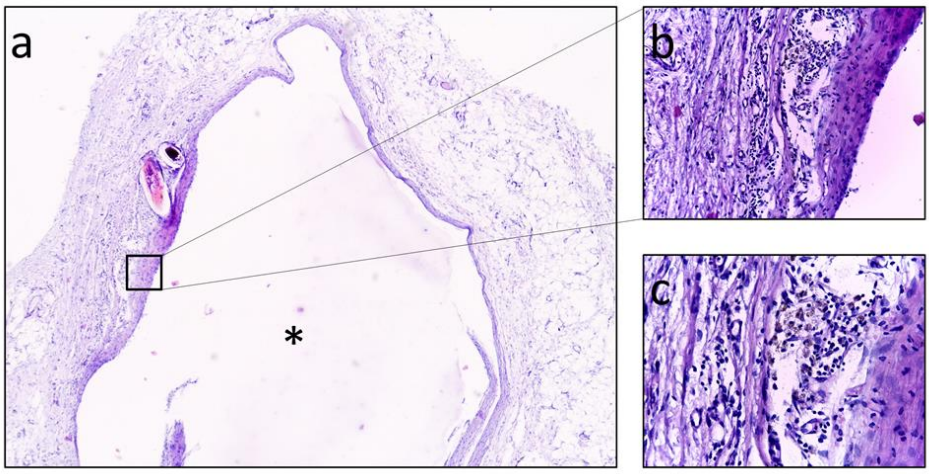

Fig.5 Subcutaneous implant with giomer sealer

* - the place where the implant was

A -4x Magnification – overview -fybroconjunctive capsule organization around the implant

B – 20x Magnification- inflammatory infiltrate Lympho- plasmocitary the most representative part

C –40x Magnification- inflammatory infiltrate Lympho- plasmocitary and minimal capillary proliferation

The most representative inflammatory cells were the lymphocytes and plasma cells, there were no macrophages found showing a moderate chronic inflammatory reaction with minimal capillary proliferation, no edema and early to partially developed capsule around the implant. Only a few giant multinuclear cells were found around A1 subcutaneous implant showing a more expressed inflammatory response. The experimental giomer sealer and Beautifil II were found moderate irritant for the subcutaneous tissue and slight irritant for the muscular tissue while the experimental restorative giomer was found moderate irritant for subcutaneous and muscular tissue. Those findings are in agreement with the biocompatibility results obtained for Beautifil II by Tamilselvam S in 2013 [44].

Capitol 6. Concluzii generale

1. Experimental restoration giomers contain original filler embedded in variable proportions in the resin matrix prepared from commercial Bis-GMA monomers (G1, G2, G3) or embedded in an original resin matrix containing an experimental analogue urethane-tetramethacrylate Bis-GMA (Bis-GMAexp) (G4, G5)
2. PRG1 and PRG2 original pre-reacted glasses were prepared by treating a superficial active glass with polyalkenoic acid P (AA-co-IA-co-Leu) or modified polyalchenoic acid grafted with methacrylic groups P (AA- IA-co-LeuM)
3. Fluorohydroxyapatite was also prepared for the original filler composition according to the method described in the literature, using thermally untreated hydroxyapatite and CaF2.
4. Four specimens of giomers used as pits and fissure sealants were also prepared using the original filler embedded into the resin matrix prepared from commercial monomers (S11, S12) or in the resin matrix containing the original monomer Bis-GMAexp (S21, S22)
5. For all the experimental giomers used for restorations SEM images revealed the relatively uniform structure in which the filler particles are fixed in the polymer matrix. In the case of commercial Bis-GMA based giomers G1 and G3, it is possible to distinguish the irregular filler particles in their structure while the giomers G4 and G5 are characterized by the superior compatibility of the hybrid filler with the original resin matrix, the filler particles appearing totally covered by the organic matrix.
6. Also for the giomer sealants, the structure investigated by SEM showed particles well fixed in the polymer matrix. Compared to the restoration giomers, a greater proportion of the polymeric matrix is observed which encloses and fixes the filler particles (present here in a lower amount than in the restoration giomers).
7. For G4 and G5 experimental restoration giomers, the conversion rate of monomers is 78.9% and 72.12% respectively, compared to 45.27%, 54.26% and 49% for G1, G2 and G3, respectively. In conclusion, the experimental giomers based on Bis-GMAexp-polymer matrix exhibit a significant improvement of conversions rate over the experimental giomers based on commercial Bis-GMA.
8. Water absorption values for G1, G2, G3 are much lower than the G4 and G5 values. The absorption of water is primarily influenced by the nature of the polymer matrix in the giomers and much less by the nature of the hybrid filler; the high values recorded for the G4 and G5 giomers are due to their composition containing the hydrophilic urethane polymer matrices.
9. The water solubility for giomers based on commercially Bis-GMA was negative: -5.09 μg / mm3 for G1, -2.83 μg / mm3 for G2 and -2.26 μg / mm3 in the case of G3 respectively. In the case of G4 and G5, the solubility recorded positive values, reaching 10, 12 μg / mm3 in the case of G5.

10. The values of the color changes of the experimental giomers exposed to coloring agents (using reflection spectra and digital image processing by means of a software application, DISCOLOR) can be well correlated; the differences not exceeding 2.0 CIELAB units (acceptable limit is 3.3 CIELAB units).
11. Among the experimental restoration giomers, the most color stable giomers were G4 and G5-the giomers based on urethane polymeric matrices.
12. When testing the mechanical properties for G5, a bending strength of 89.91 MPa was recorded, this is much higher than for the other experimental materials. Obtaining this value for bending strength is due to the presence of this bis-GMAexp monomer in the composition of the resin matrix.
13. Also, the G1, G3 and G5 giomers exhibited higher Young modulus values compared to the commercial giomer Beautifil II (Shofu), thus demonstrating from the point of view of mechanical properties the possibility of clinical use of experimental giomers materials
14. The amount of fluoride ion released by the experimental restoration giomers at day 60 is comparable to the amount of fluoride ion released from the glassionomer cements. The amount of fluoride ions released / day became similar for experimental giomers on day 60, ranging from to 1.5 ppm at 1.64 ppm, while for Beautifil II it reached half the concentration released by the experimental giomers (0.83 ppm).
15. The amount of fluoride ion released for all experimental giomers sealants exceeds the amount of fluoride ions released by the commercial product for the same period of time after 50 days of storage in distilled water, this being about twice as high in the S11 giomers and S12, and three times higher for the S21 and S22 giomers than for the Beautifil II .
16. Experimental giormers have radiopacity greater than 2mm Al, being above the limit imposed by international standard ISO 4049/2000 (1mm Al). Dental enamel has a radiopacity of 2 mm Al, and dentine, a 1 mm radiopacity of Al.
17. Of the two innovative adhesive systems (A1 and A2) developed for dental restorations to repair enamel or dentin caries by using appropriate clinical protocols, the PA2k-2-MA modified polyalchenoic acid modified adhesive system led to improved sealing at the dentin interface and a perfect adhesion to the enamel interface in the dental restorations with a giomer
18. Our findings suggest that microinfiltration in giomer restorations can be reduced by the use of a two-step adhesive based on glassionomer ionomer modified with resin containing a relatively high molecular weight polyalchenoic acid having a specific chemical formula which includes L-leucine and photopolymerizable methacrylic groups.
19. The new non-destructive investigation method of the adhesion interface by lock-in thermography characterizes the interface, being able to detect cracks or voids present along the length of the interface, both marginally and in depth. Also, this method due to noninvasive character is indicated for *in vivo* investigations of the adhesion interface.

20. Two selected S12, S22 giomer sealants were also investigated for their adhesion to enamel and the results obtained were similar to those obtained for the commercial product Fissurit F. The ideal result was obtained with the S12 giomer sealant which created a perfect seal to enamel with a good adaptation to the anatomy of occlusal pits and fissures.
21. The results obtained in testing the cytotoxicity of the experimental materials showed a decrease in cell viability by all tested biomaterials compared to the controls; the effect being dependent on their concentration and exposure time.
22. Experimental giomer biomaterials have shown similar and / or better results compared to commercial ones in *in vivo* biocompatibility testing.

Capitol 7. Bibliografie

[1] R.L. Bowen, "Development of a silica-resin direct filling material", National Bureau of Standards, Report 6333 ,1958.

[2] R.L. Bowen, "Dental filling material comprising vinyl silane-treated fused silicate and a binder consisting of the reaction product of bisphenol and glycidil acrylate", U.S. Pat., 3.066.112, 1962.

[3] W. He, R. Benson, "Handbook of Biopolymers and Biodegradable Plastics- Properties, Processing, and Applications", Chapter 5: Polymeric Biomaterials, Plastics Design Library, Edited Sina Ebnesajjad, 87-108, 2013.

[4] N. Mozner, U. Salz "New developments of polymeric dental composites", Progress in Polymer Science, **26**(4), 535-576, 2001.

[5] B. Van Meerbeek, S. Vargas, S. Inoue, Y. Yoshida, M. Peumans, P. Lambrechts, G. Vanherle, „Adhesives and cements to promote preservation dentistry", Operative Dentistry, **26**, 119-144, 2001.

[6] B. Van Meerbeek, J. De Munck, Y. Yoshida, S. Inoue, M. Vargas, P. Vijay, K. Van Landuyt, P. Lambrechts, G. Vanherle, "Buonocore memorial lecture. Adhesion to enamel and dentin: current status and future challenges", Operative Dentistry, **28**(3), 215-135, 2003.

[7] F.R. Tay, E. L. Pashley, C.Huang, M. Hashimoto, H. Sano, R.J. Smales, D.H. Pashley, "The glass-ionomer phase in resin-based restorative materials", Journal of Dental Research, **80**(9), 1808–1812, 2001.

[8] A. U. J. Yap, S. Y. Tham, L. Y. Zhu, H. K. Lee, "Short-term fluoride release from various aesthetic restorative materials" , Operative Dentistry, **27**(3), 259–265, 2002.

[9] V. Arora, P. Bogra, „Giomer, a new hybrid aesthetic restorative material," Journal of Conservative Dentistry, **5**(4), 149–155, 2002.

[10] J. D. Griffin, "Unique characteristics of the giomer restorative system", Inside Dentistry, **10**(3), 1-2, 2014.

[11] M.A.G. Gonzalez, N.H.A. Kasim, R.D. Aziz, "Microleakage Testing", Annals of Dentistry University of Malaya, **4**(1), 31-37, 1997.

[12] International Organization for Standardisation (ISO). Dental materials—testing of adhesion to tooth structure, ISO/TS 11405:2003 (E)

[13] M.A. Saghiri, K. Asgar, M. Lotfi, A.M. Saghiri, P. Neelakantan, J.L. Gutmann, A. Sheibaninia, "Back-scattered and secondary electron images of scanning electron microscopy in dentistry: a new method for surface analysis" Acta Odontol Scand, **70**(6), 603-609, 2012.

[14] S.F.C. Souza, C. Francci, A.C. Bombana, S. Kenshima, L.C. Barroso, L.C. D'Agostino, A. D. Loguercio, "Qualitative SEM/EDS analysis of microleakage and apical gap formation of adhesive root-filling materials", Journal of Applied Oral Science, **20**(3), 329-34, 2012.

[15] J.D.B. Featherstone, D. Fried, "Fundamental interactions of lasers with dental hard tissue", Medical Laser Application, **16**(3), 181-194, (2001).

[16] S. Aksakalli, A. Demir, M. Selek, S. Tasdemir, "Temperature increase during orthodontic bonding with different curing units using an infrared camera", Acta Odontologica Scandinavica **72**(1), 36-41, 2014.

[17] M. Gomes, A. Devito-Moraes, C. Francci, R. Moraes, T. Pereira, N. Froes-Salgado, L. Yamazaki, L. Silva, D. Zezell, "Temperature Increase at the Light Guide Tip of 15

Contemporary LED Units and Thermal Variation at the Pulpal Floor of Cavities: An Infrared Thermographic Analysis", Operative Dentistry, **38**(3), 324-333, 2013.
[18] G. Ja-Uk, C. Nak-Sam, "NDE of the Internal hole defect of Dental composite restoration using infared lock-in thermography", Journal of the Korean Society for Nondestructive Testing, **33**(1), 40-45, 2013.
[19] G. Ja-Uk, C. Nak-Sam, "Evaluation of Delamination of Dental Composite Restoration using Infrared Lock-in Thermography", Composite Research, **25**(6), 236-240, 2012.
[20] M. Streza, D. Dadarlat, Y. Fedala, S. Longuemart, "Depth estimation of surface cracks on metallic components by means of lock-in thermography", Review of Scientific Instruments, **84**(7), 074902, 2013.
[21] S. Sauro, R. Osorio, T.F. Watson, M. Toledano, "Assessment of the quality of resin–dentin bonded interfaces: An AFM nano-indentation, TBS and confocal ultramorphology study", Dental Materials, **28**(6), 622 – 631, 2012
[22] A.P.N. Carvalho, D.T. Dias, V.C. Bedeschi, O. Nakamura, M.Q. Oliveira, "In vitro thermal diffusivity measurements as aging process study in human tooth hard tissues", Journal of Applied Physics, **114**(19), 194705, 2013.
[23] B.M. Owens, W.W. Johnson, E.F. Harris, "Marginal permeability of self-etch and total etch adhesive systems", Operative Dentistry, **31**(1), 60-67, 2006.
[24] C.E. Dorfer, H.J. Stachle, M.W. Wurst, H. Duschner, T. Pioch,"The nanoleakage phenomenon: influence of different dentin bonding agents, thermocycling and etching time", European Journal Of Oral Sciences, **108**(4), 346-351, 2000.
[25] C. Prati, L. Tao, M Simpson, D.H. Pashley, "Permeability and microleakage of Class II resin composite restorations", Journal of Dentistry, **22**(1), 49-56, 1994.
[26] K Derhami, P Coli, M. Brannstrom, "Microleakage in class 2 composite resin restorations", Operative Dentistry, **20**(3), 100-105, 1995.
[27] C. Beznos, "Microleakage at the cervical margin of composite class II cavities with different restorative techniques" Operative Dentistry, **26**(1), 60-69, 2001.
[28] A.R. Yazici, C. Celik, G. Ozgunaltay, "Microleakage of different resin composite types", Quintessence International, **35**(10), 790-794, 2004.
[29] M.J. Tyas, M.F. Burrow, "Adhesive restorative materials: A review", Australian Dental Journal, **49**(3), 112-121, 2004.
[30] Y.Yoshida , S. Inoue, "Chemical analyses in dental adhesive technology", Japanese Dental Science Review, **48**(2), 141—152, 2012.
[31] B. Van Meerbeek, "On the development of the new bonding agents. Espertise magazine", **21**, 20-21, 2012.
[32] K. Ikemura, F.R. Tay, T. Endo, D.H. Pashley, "A review of chemical-approach and ultramorphological studies on the development of fluoride-releasing dental adhesives comprising new pre-reacted glass ionomer (PRG) fillers", Dental Materials Journal, **27**(3), 315-339, 2008.
[33] K.L. Van Landuit, J. Snauwaert, J. De Munk, M. Peumans, Y. Yoshida, A. Poitevin, E. Coutinho, S. Kazuomi, P Lambrechts, B. Van Meerbeek, "Systematic review of the chemical composition of contemporary dental adhesives", Biomaterials, **28**(26), 3757-3785, 2007.
[34] A.C. Pedreira De Freitas, L.C. Espejo, S.B. Botta, F. Sa Teixeira, M.A. Cerqueira Luz, N. Garone-Netto, A.B. Matos, M.C. Barbosa Da Silveira Salvadori, "AFM analysis of bleaching effects on dental enamel microtopography", Applied Surface Science, **256**(9), 2915–2919, 2010.

[34] M.B. Lopes, M.A. Sinhoreti, A. JR. Gonini, S. Cosani, J.F. Mc Cabe, “Comparative study of tubular diameter and quantity for human and bovine dentin at different depths”, Brazilian Dental Journal, **20**(4), 279-283, 2009.
[35] S. Habelitz, M. Balooch, S.J. Marshall, G. Balooch, G.W. Marshall, “In situ atomic force microscopy of partially demineralised human dentin collagen fibrils”, Journal of Structural Biology, **138**(3), 227–236, 2002.
[36] M.R. Carrilho, F.R. Tay, J. Sword, A.M. Donnelly, K.A. Agee, Y. Nishitani, F.T. Sadek, R.M. Carvalho, D.H. Pashley, “Dentine sealing provided by smear layer/smear plugs vs. adhesive resins/resin tags”, European Journal of Oral Sciences, **115**(4), 321–329, 2007.
[37] C. Prejmerean, D. Prodan, M. Vlassa, M. Sreza, T. Buruiana, L. Colceriu, V. Prejmerean, S. Cuc, M. Moldovan, “ATR technique an appropriate method for determining the degree of conversion in dental giomers”, Measurement Science and Technology, **27**(12), 124008, 2016.
[38] M. Streza, I. Hodisan, C. Prejmerean, C. Boue, G. Tessier, “Lock-in thermography, penetrant inspection, and scanning electron microscopy for quantitative evaluation of open micro-cracks at the tooth-restoration interface”, Journal of Physics D: Applied Physics, **48**(10), 105401, 2015.
[39] J. Leirskar, K. Helgeland, “Mechanism of toxicity of dental materials”, International Endodontic Journal, **14**, 42-48, 1981.
[40] International Organization for Standardisation (ISO). Biological evaluation of medical devices. ISO 10993-6:2007
[41] E. Bodrumlu, M. Muglali, M. Sumer, T. Guvenc, “The response of subcutaneous connective tissue to a new endodontic filling material”, Journal of Biomedical Materials Research Part B: Applied Biomaterials, **84**(2), 463-467, 2008.
[42] B. Swetha, S. Mathew, B.V. Sreenivasa, N. Shruthi, S.H. Bhandi, “Determination of biocompatibility: A review”, International Dental &Medical Journal of Advanced Research, **1**, 1-6, 2015.
[43]M.S. Botsali, A. Kusgoz, S.H. Altintas, H. E. Ülker, M. Tanriver, S. Kiliç, F. Başak, M. Ülker, “Residual HEMA and TEGDMA release and cytotoxicity evaluation of resin-modified glass ionomer cement and compomers cured with different light sources”, Scientific World Journal, ID 218295, 2014
[44] S. Tamilselvam, M.J. Divyanand, P. Neelakantan, “Biocompatibility of a Conventional Glass Ionomer, Ceramic Reinforced Glass Ionomer , Giomer and Resin Composite to Fibroblasts: in vitro Study”, Journal of Clinical Pediatric Dentistry, **37**(4), 403-406, 2013.